NAG W-91

Univ. of Colorado
Boulder, Colorado

Quenching of the Beam-Plasma Instability by 3-D Spectra of Large Scale Density Fluctuations

L. Muschietti, M.V. Goldman, and D. Newman

September 1984

Abstract

A model is presented to explain the highly variable yet low level of Langmuir waves measured in situ by spacecraft when electron beams associated with Type III solar bursts are passing by; the low level of excited waves allows the propagation of such streams from the sun to well past 1 AU without catastrophic energy losses. The model is based, first, on the existence of large scale density fluctuations that are able to efficiently diffuse small-k beam-unstable Langmuir waves in phase space, and, second, on the presence of a significant isotropic non-thermal tail in the distribution function of the background electron population, which is capable of stabilizing larger k modes. The strength of the model lies in its ability to predict various levels of Langmuir waves depending on the parameters. This feature is consistent with the high variability actually observed in the measurements. The calculations indicate that, for realistic parameters, the most unstable, small k modes are fully stabilized while some oblique mode with higher k and lower growth rate might remain unstable; thus a very broad range of levels of Langmuir waves is possible from levels of the order of enhanced spontaneous emission to the threshold level for nonlinear processes. On the other hand, from in situ measurements of the density fluctuations spectrum by ISEE 1 and 2 in the vicinity of the earth, it is shown that measured 100 km scale fluctuations may be <u>too</u> effective in quenching the instability. If such strong density fluctuations are common in the solar wind, we show they must be highly anisotropic in order to allow the build-up of Langmuir waves to the observed mV/m range. Moreover, the anisotropy must be such that the strongest variations of density occur in a plane perpendicular to the magnetic field.

1. Introduction

Highly variable yet rather low levels of Langmuir waves have been measured in situ by spacecraft when electron-beams associated with Type III solar bursts are passing by; due to the low level of excited waves the propagation of such streams from the sun to well past 1 AU is possible without catastrophic energy losses. Detailed measurements at 1 AU (Lin et al., 1981) have shown clearly the simultaneous occurrences of a bump on tail electron distribution function and a rise of plasma waves above the background level. Yet they also reveal that this distribution remains for a long enough time ($t \approx 10$ min) to drive the plasma waves to far higher levels (according to linear instability theory) than the maximum values observed of a few mV m^{-1} and that, contrary to what might be expected from pure quasilinear theory, no plateau formation of the distribution is evident. One possible explanation is that various nonlinear wave-wave interactions such as decay instability, OTS, modulational instability, and soliton collapse are effective in limiting the wave growth by shifting the waves out of resonance with the beam (Weatherall et al., 1981; Grognard, 1982). It should be noted, nevertheless, that the threshold for such nonlinear processes to occur is about 10 mV m^{-1} for conditions prevailing at 1 AU.

On the other hand, the electron density has been observed to fluctuate significantly in the solar wind. In situ measurements of the density fluctuation spectrum by ISEE 1 and 2 (Celnikier et al., 1983) reveal that a variation $\delta n/n$ as high as 10^{-2} may exist on the 100 Km scale range in the vicinity of the Earth, while observations of interplanetary scintillation from extragalactic radio sources (Cronyn, 1972) lead to an average value $\delta n/n$ of

the order of 10^{-3} (Smith and Sime, 1979). Thus it seems that the background density of the solar wind, although not precisely known, is far from being homogeneous and that, when dealing with the Langmuir turbulence associated with Type III bursts, typically at Km wavelength, the effect of the inhomogeneities must be accounted for. In this paper we show that the large scale density fluctuations may be extremely effective in shifting the waves out of resonance with the beam and therefore in quenching the instability. Following an idea studied by Nishikawa and Ryutov in the context of laboratory relativistic electron beams (Nishikawa and Ryutov, 1976) and by Goldman and DuBois in that of the solar wind (Goldman and DuBois, 1982), it is hypothesized that the effect of the inhomogeneities on the Langmuir turbulence may be treated in terms of a diffusion process in phase space. However, unlike the latter authors, we take into account the non-Maxwellian background electron distribution, which results in quite different spectra, and we do not assume that the background density fluctuations are necessarily isotropic. In fact, it will be shown that, if the high level of density fluctuations measured by ISEE is common and of long duration, the fluctuations must indeed be highly anisotropic in order to allow the build-up of Langmuir waves up to the mV/m range. Moreover, the anisotropy must be such that the strongest variations of density occur in a plane perpendicular to the magnetic field. This feature leads to a picture of the solar wind as composed of structures elongated along the magnetic field axis in a way consistent with the ducting considerations invoked by experts in radio-wave propagation (Robinson, 1983; Duncan, 1979; Bougeret and Steinberg, 1977).

2. Model

A heuristic picture of the wave diffusion process may be outlined briefly for the reader familiar with particle velocity space diffusion (i.e. quasilinear Vlasov theory). In the Langmuir wave diffusion, the plasmon (of wavenumber k) plays the role of a diffusing particle in the usual quasilinear Vlasov theory and the role of the external potential is played by the varying refractive index associated with the density fluctuations (with a spectrum of wavenumbers characterized by q). Suppose $q^{-1} < L_g$ where L_g is the typical growth length of the Langmuir waves so that a spectral energy density averaged in space $W(\underline{k})$ may be used. Further, we assume $q << k$; then the relative change of $\underline{k}$ is small in each scattering event and the process is treated as a diffusion. The diffusion in k-space experienced by the plasmon may be estimated as $D \approx k^{-2} |\frac{dk}{dt}|^2 t_{ac}$ with $\frac{dk}{dt}$ the fluctuating force acting on it for an autocorrelation time t_{ac}. Since $\frac{dk}{dt} = -\frac{\partial \omega_{pe}}{\partial x} \approx \omega_{pe} \delta n/n \, q$, and t_{ac} is of the order of the transit time for the plasmon across one density fluctuation, $t_{ac} \approx (qV_g)^{-1} \approx (qk\lambda_D v_e)^{-1}$, we have $D \approx \omega_{pe} (q/k) (k\lambda_D)^{-2} (\delta n/n)^2$.

A more rigorous general theoretical derivation (Goldman and DuBois, 1982) leads, with the above assumptions, to the following Fokker-Planck equation for the spectral energy density of Langmuir waves in phase space.

$$\partial_t W_k = 2\gamma_k W_k + \partial_{k_j} D_{j\ell} \partial_{k_\ell} W_k + S_k \qquad (1)$$

where the diffusion coefficient is

$$D_{j\ell} = \omega_{pe} \pi \int d^3q/(2\pi)^3 \, C(\underline{q}) \, q_j q_\ell \, \delta(2\underline{k}\cdot\underline{q}) \qquad (2)$$

and $C(\underline{q})$ is the spectrum of density fluctuations:

$$\int d^3q/(2\pi)^3\ C(\underline{q}) = (\delta n^2/n^2)\ . \tag{3}$$

The diffusion coefficient, Equation (2), incorporates the assumption of elastic scattering. That assumption is justified when the propagation velocity of the density inhomogeneities is small as compared to the group velocity of the plasmon $V_g = 3\ k\lambda_D v_e$. Note that in Equation (1) we have added an electron spontaneous emission term S_k.

By assuming that the problem displays an azimuthal symmetry around the beam axis we may rewrite Equation (1) as

$$\partial_t\ W(k,\theta) = 2\nu_k\ W(k,\theta) + (\sin\theta)^{-1}\partial_\theta\ D(k,\theta)\ \sin\theta\ \partial_\theta W(k,\theta) + S(k,\theta) \tag{4}$$

where $D(k,\theta)$ is derived from Equation (2):

$$D(k,\theta) = \omega_{pe}^3/v_e^2\ 1/k^3\ 1/(12\pi^2)\ \Omega(\theta) \tag{5}$$

with

$$\Omega(\theta) = \int d(\cos\bar{\theta})\ \bar{C}(\bar{\theta})\ \frac{\cos^2\bar{\theta}/\sin^2\theta}{(\sin^2\theta\sin^2\bar{\theta}-\cos^2\theta\cos^2\bar{\theta})^{1/2}} \tag{6}$$

where $\bar{C}(\bar{\theta}) = \int dq\ q^3\ C(q,\bar{\theta})$ and I is the domain $\cos\bar{\theta} < |\sin\theta|$.
Note that the diffusion occurs in angle only as a result of the assumption of elastic scattering.

The growth rate (or damping) γ_k and the spontaneous emission term S_k in Equation (4) depend on the actual distribution function. We model them by

$$f(\underline{v}) = n/(2\pi v_e^2)^{3/2} \exp(-v^2/2v_e^2) + n_T\, 5v_T^5/4\pi\, v^{-8}\, H(v-v_T) + n_b/(2\pi)^{3/2}\, \Delta v^{-3} \exp[-(\underline{v}-\underline{v}_b)^2/2\Delta v^2] . \quad (7)$$

Here H is the Heaviside step function, n_T and n_b are the fractions of electrons in an observed non-thermal electron tail and in the beam feature (relative to the bulk); Δv is the beam velocity spread. The shape of the tail simulates a non-thermal component, such as that observed by Lin et al. (1981) prior to and after the passage of the beam. We assume that it is valid down to a velocity $v = v_T \approx 5v_e$. Since the beam velocity $v_b \approx 60\text{-}90\ v_e$, waves with a phase velocity $v_{ph} < 5v_e$ will not be considered. Then the presence of a step at v_T in the distribution function has no importance, and a smooth matching of the tail to the bulk is not required. It should be mentioned here that attempts have been made to simulate the slight measured anisotropy of the tail associated with a heat flux (Gurnett et al., 1979); these have not led to significantly different results of concern to us, so that complication will be omitted in the following.

The growth/damping rate γ_k consists thus of two isotropic terms due to the Landau damping from the bulk velocity distribution (denoted by M for Maxwellian) and from the tail (denoted by T)

$$\gamma^{(M)} = -(\pi/8)^{1/2}\, \omega_{pe}/(k\lambda_D)^3 \exp[-1/2\,(1/k\lambda_D)^2] \quad (8a)$$

$$\gamma^{(T)} = -5\pi/4\ \omega_{pe}\ n_T\ (v_T/v_e)^5\ (k\lambda_D)^5 \tag{8b}$$

and of an anisotropic term due to the beam

$$\gamma^{(b)} = (\pi/8)^{1/2}\omega_{pe}^3 n_b/\Delta v^3 1/k^2(v_b\ \cos\theta-\omega_{pe}/k)\exp[-1/2\Delta v^2(v_b\ \cos\theta-\omega_{pe}/k)^2] \tag{8c}$$

Similarly, the spontaneous emission is composed of two isotropic and one anisotropic term

$$S^{(M)} = -2\gamma^{(M)}\ mv_e^2\ , \tag{9a}$$

$$S^{(T)} = (5\pi/12)\ \omega_{pe}^{-2}\ mv_T^2\ n_T\ (kv_T)^3\ , \tag{9b}$$

$$S^{(b)} = (\pi/2)^{1/2}\ \omega_{pe}^2\ m(\omega_{pe}/k)^2\ n_b/k\Delta v\ \exp\ [-\ 1/2\Delta v^2\ (v_b\cos\theta\ -\ \omega_{pe}/k)^2] \tag{9c}$$

When the rate of diffusion of the Langmuir waves out of unstable regions into stable regions of the phase space is high enough, Equation (4) has a stationary solution. In order to study the stability boundaries in parameter space as well as the level of electric field, Equation (4) has been solved numerically in the steady state limit for various parameters.

3. Results and Interpretation

3.1 Numerical Results

The Fokker-Planck Equation (4) displays two kinds of solution. Either the rate of diffusion of the Langmuir waves out of unstable regions into dissipation regions of the phase space is rather small and the wave energy grows up ad infinitum as in the usual linear theory, or the rate is high enough in order that the wave energy saturates, and Equation (4) then has a steady solution.

A typical steady solution may be seen in Figure 1. Figure 1a displays the contours of the wave energy density spectrum W_k/T_e in the k-θ plane of phase space. Note that the enhanced spontaneous emission due to the non-thermal tail, $W_k/T_e \approx S^{(T)}/(-2\gamma^{(T)}T_e)$, would lead (with the parameters of the Figure) to a spectrum of order 10^2 in the region of phase space displayed. Thus, because of the diffusion, even the backward propagating damped modes ($\theta > \pi/2$) have a comparatively high level of wave energy. Let us now consider the total electric field associated to a steady solution.

3.2 Properties of Steady State Solutions

On a sphere of radius k in three-dimensional $\underline{k}$-space, energy source regions are connected to energy sink regions by angular diffusion. Therefore, it is possible to write a balance equation after integrating Equation (4) on the sphere. For that purpose we define the two averages

$$\langle \gamma_k \rangle = 1/\bar{W}_k \int_{-1}^{+1} d(\cos\theta)\ \gamma_k(\theta)\ W(k,\theta) \qquad (10)$$

where $$\bar{W}_k = \int_{-1}^{+1} d(\cos\theta)\, W(k,\theta) \quad ,$$

and

$$\bar{\gamma}_k = 1/2 \int_{-1}^{+1} d(\cos\theta)\, \gamma_k(\theta) \quad . \tag{11}$$

Since the angle average of the diffusion term vanishes, the balance equation may be written as

$$\bar{W}_k = \bar{S}(k)/(-2\langle\gamma_k\rangle) \quad . \tag{12}$$

Where the diffusion coefficient $D(k,\theta)$ is large, a very weak angular gradient in the spectrum is sufficient for the diffusion flux to remove the wave energy from regions of sources into regions of sinks. The spectrum is therefore approximately independent of θ so that $\langle\gamma_k\rangle = \bar{\gamma}_k$. A key point of Nishikawa and Ryutov (1976) was to show that $\bar{\gamma}_k<0$ for any distribution irrespective of the presence of a beam. Where $D(k,\theta)$ is weaker, the spectrum begins to peak in angle at the energy source regions where $\gamma_k(\theta)>0$.

This can be seen from numerical solutions to the steady state diffusion equation. In one such solution, shown in Figure 1a, the Langmuir energy has piled up in the forward propagating modes ($\theta<\pi/2$) which are in Cerenkov resonance with the positive slope of the beam. Figure 1b displays clearly the angular gradient of the spectrum that may occur at some wavenumbers. As a result of this spectral behaviour, the weighted average defined by Equation (10) emphasizes the contribution from the forward angles, for which $\gamma_k(\theta)>0$, in

relation to the wider angular range, for which $\gamma_k(\theta)<0$. By contrast, in the average, $\bar{\gamma}_k$, all angles are weighted equally. Therefore

$$\bar{\gamma}_k << \gamma_k > \qquad (13)$$

This inequality becomes stronger for more highly peaked spectra. In fact, $<\gamma_k>$ may go through zero, in which case a physical steady state solution (cf. Equation (12)) no longer exists, (i.e. the growing Langmuir waves cannot be saturated.) A discussion about marginal stability is deferred to the next section.

Let us assume here that $<\gamma_k><0$. Then combining Equations (12) and (13) one has

$$\bar{W}_k > \bar{W}_k^{min} = \frac{\bar{S}^{(b)}+S^{(T)}+S^{(M)}}{-2(\bar{\gamma}^{(b)}+\gamma^{(T)}+\gamma^{(M)})} \qquad (14)$$

where $\bar{W}_k^{min}$ may be easily calculated from Eqs. (8)-(9) and evaluated for various parameters. $\bar{W}_k^{min}$ turns out to be comparable in magnitude to $\bar{W}_k$. In Table I values of $\gamma_{max}^{(b)}$, $\bar{\gamma}^{(b)}$, $\gamma^{(T)}$, $\bar{S}^{(b)}$, $S^{(T)}$ and $\bar{W}_k^{min}/T$ are reported over a range of wavenumbers for the "nominal" beam and tail parameters.

When one compares the level of Langmuir waves determined by spontaneous emission without the beam to $\bar{W}_k^{min}$, one notices that the angle-averaged spectral energy density is substantially enhanced due to the beam over a range of small wavenumbers only where the tail is not important; from Table I and Equation (14) it is seen that above $k\lambda_D = 5\cdot10^{-2}$ the beam does not play any

role. Thus, even if the beam-resonant spectral energy density, $\bar{W}_k/T$, is enhanced by as much as 10^4 through optimum choice of parameters, the effect on the <u>total</u> energy density is very weak. An upper bound to the enhancement of the energy density would be

$$\int_{10^{-2}}^{5\times10^{-2}} d(k\lambda_D)(k\lambda_D)^2/(2\pi^2) \cdot 10^4/n\lambda_D^3 = 2\cdot10^{-2}/n\lambda_D^3$$

so that the total energy density would be $E^2/(4\pi nT) = 5\cdot10^{-2}/n\lambda_D^3$ and the electric field only 1.5 μV/m for the solar wind parameters at 1 AU ($n = 10\ cm^{-3}$, $\lambda_D = 8m$, $T = 13\ eV$). This is, of course, far too small to account for the observations. We are led to conclude that the rise of plasma waves measured when the beam arrives is not due to an enhancement of the spontaneous Langmuir fluctuations as implied by Equation (14) but to growing waves which cannot be saturated by the processes considered.

A comment should be made about the results obtained in a previous study (Goldman and Dubois, 1982). In that study the role of the electron tail was not considered, so that the beam enhanced modes could extend up to $k\lambda_D = 0.15$, which resulted in an enhancement of the total energy density of two orders of magnitude, and an enhancement of one order for the electric field.

3.3 Criterion for Steady State Solutions in the Presence of Isotropic Density Fluctuations

When the density fluctuations are isotropic, Equation (6) is easily integrated, and the diffusion coefficient takes a form which is independent of θ:

$$D_{iso} = \omega_{pe}/24\pi\ (1/k\lambda_D)^2\ 1/k \int dq\ q^3\ C(q)$$
$$= \pi/12\ \omega_{pe}/(k\lambda_D)^2\ \bar{q}/k\ \langle \delta n^2/n^2 \rangle$$
$$= D_o/(k\lambda_D)^3 \quad , \tag{15}$$

where $\bar{q}$ is a typical wavenumber associated with the fluctuations. Due to the k^{-3} dependence, it is expected that unstable modes with a high phase velocity will be more quickly diffused out of the unstable region than will lower phase velocity modes. Thus, the quenching of the instability by the density fluctuations is expected to be much more effective for the high phase velocity waves. In fact, this difference in behaviour is even more pronounced because of the angular dependence of the Langmuir spectrum at different k. That feature should become clear for the reader from the following model.

Let us consider the energy source and sink angular regions determined by the beam on a sphere of fixed radius k. For that purpose we rewrite Equation (8c) and Equation 9(c) in terms of the variable $x = \cos\theta$ with k considered as a parameter

$$\gamma^{(b)}(x) = (\pi/8)^{1/2}\ n_b v_b/\Delta v^3\ \omega_{pe}^2/k^2\ (x - \omega_{pe}/kv_b)$$
$$\times \exp\left[-v_b^2/2\Delta v^2\ (x-\omega_{pe}/kv_b)^2 \right] \tag{16}$$

$$S^{(b)}(x) = (\pi/2)^{1/2}\ n_b \omega_{pe}^2/k\Delta v\ m(\omega_{pe}/k)^2$$
$$\times \exp\left[-v_b^2/2\Delta v^2\ (x-\omega_{pe}/kv_b)^2 \right] \tag{17}$$

The behaviour of the above expressions is characterized by three particular

angles: $x_o = \omega_{pe}/kv_b$ where $\gamma^{(b)}(x_o) = 0$ and $S^{(b)}(x_o)$ is maximum, $x_M = \omega_{pe}/kv_b + \Delta v/v_b$ where $\gamma^{(b)}(x_M)$ is maximum, and $x_m = \omega_{pe}/kv_b - \Delta v/v_b$ where $\gamma^{(b)}(x_m)$ is minimum.

In the region $x_o<x<1$ one has the power input

$$P_{in} = 4\pi \int_{x_o}^{1} \gamma^{(b)}(x)\, W(x)dx + \sigma^{+} \tag{18}$$

with $\sigma^{+} = 2\pi \int_{x_o}^{1} S^{(b)}(x)dx > 0$

while in the region $-1<x<x_o$ one has the power output

$$P_{out} = -4\pi \int_{-1}^{x_o} \gamma^{(b)}(x)\, (x)\, dx - \sigma^{-} \tag{19}$$

with $\sigma^{-} = 2\pi \int_{-1}^{x_o} S^{(b)}(x)\, dx > 0.$

One necessary condition for stability is

$$P_{in} = P_{out} \tag{20}$$

On the other hand, the flux of energy from one region to the other,

$$\Phi = 2\pi(1-x_o^2)\, D(x)\, \frac{dW}{dx}\Big|_{x_o} = 2\pi\, D_o\, (v_b/v_e)^3 x_o^3\, (1-x_o^2)\, \frac{dW}{dx}\Big|_{x_o} \tag{21}$$

must balance the input of power,

$$\Phi = P_{in} \quad . \tag{22}$$

which represents a second requirement for stability.

In order to form analytic criteria for steady state, we now model the spectral shape, according to our numerical experiments, by a Maxwellian centered on axis and a flat background (cf. the numerical result in Figure 1b for an example):

$$W(x) = W_m + \Delta W \exp\left[-\tfrac{1}{2} \left((x-1)/(x_o-1)\right)^2 \right] \quad . \tag{23}$$

with the two free parameters W_m adn ΔW. Then we may rewrite Equation (20) as (the detailed calculations are left for the Appendix)

$$SF \leq 1.17/\left[1-\exp\left[-v_b^2/2\Delta v^2(1-x_o)^2\right] \right] - 0.17 \tag{24}$$

where the swelling factor SF is defined as the ratio of the peak to bottom values of the spectrum $SF = 1 + \Delta W/W_m$.

Thus the very fact that the energy sink and source angular regions are finite on the sphere of radius k, and in a definite ratio, leads to a maximum bound of the swelling factor. As the marginal stability boundary is approached, the spontaneous emission becomes negligible and SF is equal to its maximum bound. Now, as the wavenumber k increases, $x = \omega_{pe}/kv_b$ decreases so that the maximum bound decreases too (cf. Equation (24)). The spectrum is not allowed to be as highly peaked for large k as it is for small k. However, a certain amount of peaking is required in order for the flux Φ to balance the input of power: Equation (22) leads to (cf. Appendix for details)

$$SF \geq 1 + \left\{ \frac{0.48\ D_o/\omega_{pe}(v_b/\Delta v)^3 x_o(1+x_o)}{n_b(v_b/\Delta v)\ \left[1-\exp[-(v_b^2/2\Delta v^2)(1-x_o)^2]\right]} - 0.85 \right\}^{-1} \tag{25}$$

Let us define for a given wavenumber k,

$$\gamma_{max}^{(b)} = \gamma^{(b)}(x_M) = (\pi/8e)^{1/2}\ n_b\omega_{pe}^3/(k\Delta v)^2 \quad . \tag{26}$$

Combining the inequalities (24) and (25), an upper bound on $\gamma_{max}^{(b)}$ for a steady state solution to exist may be written as

$$\gamma_{max}^{(b)} \leq \tilde{\Gamma}_{crit}(x_o) \tag{27}$$

with

$$\tilde{\Gamma}_{crit}(x_o) = 0.22\ \frac{(v_b/v_e)^3(v_b/\Delta v)\ x_o^3(1+x_o)}{\exp[-(v_b^2/2\Delta v^2)(1-x_o)^2] - 1} \tag{28}$$

From the viewpoint of numerical solutions of the diffusion equation it is possible, for a given k or x_o, to increase $\gamma_{max}^{(b)}$ by increasing the strength of the beam n_b to a <u>numerically</u> determined maximum value, $\Gamma_{crit}(x_o)$, where the marginally stationary boundary is reached and beyond which the spectrum grows without (linear) bound. Due to the exponential dependence in x_o displayed by the RHS of inequality (27) $\Gamma_{crit}(x_o)$ is expected to fall-off very rapidly with increasing k.

In Figure 2 the exact Γ_{crit} obtained by the numerical solution of Equation (4) for given sets of parameters characterizing the beam has been

plotted as a function of $kv_b/\omega_{pe} = 1/x_o$. The agreement with the expression for $\tilde{\Gamma}_{crit}$ given in (28) is satisfying. The rapid fall-off with increasing wavenumbers or decreasing phase velocities is evident. By comparing with the relatively slow k^{-2} decrease of $\gamma_{max}^{(b)}$ one sees that, even if the small k modes with the supposedly largest growth rate are stabilized because, for those k, $\Gamma_{crit} > \gamma_{max}^{(b)}$, for larger k the inequality may be reversed so that the beam instability is then only partially stabilized. Two important points are worth stressing about those "residual" unstable waves. As compared to the fastest growing k-mode with phase velocity $\omega_p/k = v_b - \Delta v$ and $\theta = 0$, they have a smaller growth rate given by Equation (26) and are oblique, $\cos\theta = x_M < 1$.

Let us now turn to the role played by the nonthermal tail. In the first place, the associated damping $\gamma^{(T)}$ increases quickly with increasing wave number (cf. Equation (8b)). Due to that, the stability boundary, Γ_{crit}, takes a V-shape as plotted in Figure (3). The second effect caused by the tail is less transparent. It may be understood however following the same line of reasoning as before. On a sphere of radius k the nonthermal tail reduces both the energy source region and the strength of the source; correlatively the energy sink region as well as the strength of the sink is increased. This gives rise to a greater peaking of the spectrum. The flux of energy from the source area to the sink area can then be more important. Therefore, the input of power can be raised, so that Γ_{crit} is upshifted. For the plot we have used a diffusion coefficient $D_o = 8 \cdot 10^{-12} (k\lambda_D)^{-3}$; it corresponds to a fluctuation level of $\delta n/n = 5 \cdot 10^{-4}$ in the range q^{-1}=100 km, which is low compared to levels measured by ISEE. The parameters of the tail have been fitted from the non-Maxwellian component observed by Lin et al. (1981), $n_T(v_T, v_e)^5 = 20$. In that situation a beam of parameters $n_b = 5 \cdot 10^{-7}$,

v_b/v_e=90, $\Delta v/v_e$=20, is completely stabilized (cf. $\gamma^{(b)}_{max}$ in dashed line). Yet, were the beam 40% denser, n_b=7·10^{-7}, a small range of k would be unstable (dotted line).

In general, three different regions of k-space must be considered. In the small k region, $k<k_1$, $\gamma^{(b)}$ is stabilized by the diffusion. k_1 may be expressed by using Equation (28) for evaluating Γ_{crit} in the condition

$$\tilde{\Gamma}_{crit}(k_1) = \gamma^{(b)}_{max}(k_1)$$

Let $x_1 = \omega_{pe}/k_1 v_b$; by means of Equation (26) one may obtain the implicit equation for x_1

$$x_1 = 1 - \sqrt{2\Delta v/v_b}\ \left\{ \mathrm{Ln}\left[1 + 0.58\ D_o/\omega_{pe} v_b^2 \Delta v/v_e^3\ 1/n_b\ x_1(1+x_1) \right] \right\}^{1/2} \qquad (29)$$

In the high k region, $k>k_2$, $\gamma^{(b)}$ is stabilized by $\gamma^{(T)}$. k_2 is defined by

$$\gamma^{(T)}(k_2) = -\gamma^{(b)}_{max}(k_2)$$

or, using Equations (8b) and (26)

$$k_2 \lambda_D = (0.10\ n_b v_e^5/n_T v_T^5\ v_e^2/\Delta v^2)^{1/7} \qquad (30)$$

In the intermediate region, $k_1<k<k_2$, there might remain weakly unstable modes so that the beam instability is only partially quenched and therefore slowly growing electric fields are present. Then, either the instability saturates

because of some weak nonlinearity such as decay off ions, or simply because after a while ($t \approx 10$ min) the waves enter in Cerenkov resonance with the negative slope of the beam due to the advection of the latter. Depending on the actual parameters, the relative position of the two curves Γ_{crit} and $\gamma_{max}^{(b)}$ may change so that various growth rates, and therefore levels of measured electric fields, are expected. In Figure 4 we display the change of Γ_{crit} brought about by: a) an increase in the level of density fluctuations; b) a downshift of the beam velocity and c) a decrease in the strength of the tail. For comparison the Γ_{crit} of Figure 3 is indicated with a dashed line.

We are now ready to write a sufficient criterion for linear saturation by letting $k_1 > k_2$ and using Equation (29)

$$k_2 v_b - \sqrt{2} k_2 \Delta v \left\{ \ln \left[1 + 0.58 \, (D_o/\omega_{pe})(\Delta v/v_e) \frac{k_2 v_h + \omega_{pe}}{\omega_{pe} n_b (k_2 \lambda_D)^2} \right] \right\}^{1/2} < \omega_{pe} \qquad (31)$$

where k_2 may be computed via Equation (30).

It is important to note that when the strong level of density fluctuations actually measured by ISEE is used to evaluate the coefficient D_o ($D_o = 10^{-8} \omega_{pe}$), the above inequality is satisfied for any conceivable beam associated with Type III bursts. Thus, the instability is definitely saturated linearly by the diffusion process.

3.4 Anisotropic Density Fluctuations; the Quest for Instability

At the end of Section 3.2 it was shown that the level of electric field is hardly raised above background when dealing with steady state solutions to the

diffusion equation. On the other hand, it has just been claimed that the density fluctuations measured by ISEE were so strong that a steady state solution is justified. Therefore, we are faced with a dilemma: either the 3 hour measurements on September 8, 1978 by ISEE were quite exceptional and not at all representative of the usual solar wind, or something is basically wrong in the model developed. We suspect that the difficulty lies with one assumption which is not supported by observational evidences: the assumed isotropy of the density fluctuations.

Let us assume that the density fluctuations split into two regions (cf. Figure 5a)

$$\bar{C}(\bar{\theta}) = \begin{cases} C_{\parallel} & |\cos\bar{\theta}| > \alpha \\ C_{\perp} & |\cos\bar{\theta}| < \alpha \end{cases} \qquad 0 < \alpha = \cos\theta_o < 1$$

Then Equation (6) may be easily integrated to yield

$$\Omega(\theta) = H(\alpha-\sin\theta)\, C_{\perp}\pi/2 + H(\sin\theta-\alpha)\left\{C_{\parallel}\pi/2+(C_{\perp}-C_{\parallel})\left[\mathrm{Arcsin}(\alpha/\sin\theta)-\alpha/\sin\theta(1-\alpha^2/\sin^2\theta)^{1/2}\right]\right\} .$$

In case of isotropic density fluctuations with the same energy one obtains

$$\Omega_{iso} = \pi/2\,[C_{\parallel} + \alpha(C_{\perp}-C_{\parallel})] \quad .$$

Therefore, the relative reduction of the diffusion coefficient $\Omega(\theta)/\Omega_{iso}$ may be evaluated at some angles.

Let us imagine for example that the fluctuations are concentrated in a plane perpendicular to the beam axis, $C_{||} = 0$, $\alpha \ll 1$ (cf. Figure 5c). Then $\Omega(\pi/2)/\Omega_{iso} = 2\alpha^2/3 \ll 1$, namely the forward propagating modes are nearly isolated from the backward ones. The forward modes are generally destabilized by the beam whereas the backward ones are always damped so that the unstable domain of phase space is cut off from the one of absolute damping, and the beam instability may not be expected to be completely quenched. On the other hand, if the fluctuations are concentrated along the beam axis, $C_{\perp} = 0$, $\alpha \lesssim 1$ (cf. Figure 5b), one has $\Omega(o)/\Omega_{iso} = 0$, namely the parallel modes do not experience any diffusion at all and growth persists. Of course, from a physical point of view, since the beam axis coincides with the magnetic field axis and because the diffusion of the plasma particles is inhibited by the magnetic field, the inhomogeneities in density are more likely to be oriented across rather than parallel to the axis.

In view of that we introduce the following model of anisotropic density fluctuations

$$C(q,\theta) = p(q)\ a/\pi\ (\cos^2\theta+a^2)^{-1} \qquad a \ll 1 \tag{32}$$

where $p(q)$ is determined from the ISEE 1-2 experiment (Celnikier et al., 1983)

$$p(q) = 2.5\ 10^{-6}\ (q\lambda_D)^{-2.9} \qquad 9\cdot10^{-6} < q\lambda_D < 7\cdot10^{-4}\ .$$

By substituting Equation (32) into Equation (6) one obtains

$$\Omega(\theta) = 7.6\ 10^{-10}\ \ a/\sin^2\theta\ \left[\,1 - a/(a^2+\sin^2\theta)^{1/2}\,\right]\ .$$

Thus the diffusion coefficient (Equation (5)) reads

$$D(k,\theta) = 6.4\ 10^{-9}\ \omega_{pe}\ (1/k\lambda_D)^3\ a/\sin^2\theta\ \left[\,1 - a/(a^2+\sin^2\theta)^{1/2}\,\right] \quad . \qquad (33)$$

The Fokker-Planck equation has been solved numerically using this diffusion coefficient. In Figure 6 it may be seen that the anisotropy in the density fluctuations leads to a concentration of the Langmuir energy in the forward propagating modes. Now, if the anisotropy is pronounced enough, the flux of energy at large angles between the source and sink regions may be too small to balance the power generated. The largest angle we have to consider is given by $\cos\theta = \omega_p/k_2 v_b$ where k_2 is defined in Equation (30). On the other hand, it has been shown in Sec. 3.2 that with the parameters, $n_b = 10^{-6}$, $v_b = 90\ v_e$, $\Delta v = 20\ v_e$ and $n_T(v_T/v_e)^5 = 20$ a diffusion coefficient $D_{iso} = 8\cdot10^{-12}(k\lambda_D)^{-3}$ is too small to provide enough diffusion to quench the instability. Therefore, we may expect to recover this situation for $a < 8\cdot10^{-12}/6.4\ 10^{-9}\cdot(1-(\omega_p/k_2 v_b)^2) = 10^{-3}$. The numerical integration of the Fokker-Planck equation indeed shows that for $a < 5\cdot10^{-4}$ the fluctuations are unable to quickly remove the Langmuir energy from the beam unstable region of the phase space, and the wave develops unstably in spite of the strong general level of density fluctuations. Only in this case, may electric fields in the mV/m range be expected (consistently with observations). Thus, although measurements of both electric fields in the mV/m range and electron density fluctuations in the 10^{-2} range have not been obtained simultaneously, our results strongly suggest that such density inhomogeneities of the solar wind must be elongated along the magnetic field.

4. Conclusion

This study of the role played by the large scale density fluctuations of the solar wind in relation to TIII electron streams leads to the following conclusions.

1) It is possible to understand the rather low level, intermittent character of the beam-excited Langmuir waves observed in situ, by considering the background density fluctuations. In an environment where the latter are strong and isotropic, the growth of Langmuir waves is quenched and the electric field is hardly raised above its background value. However, when the density fluctuations are smaller, slowly growing Langmuir waves are present, which may result in an electric field in the mV/m range.

2) Another explanation for the mV/m Langmuir fields observed is as follows: If the relatively small scale density inhomogeneities of the solar wind ($\delta n/n \sim 10^{-2}$, $q^{-1} \sim 10^{2}$ kms) are assumed to be highly anisotropic and elongated along the magnetic field in a way consistent with the large inhomogeneities ($\delta n/n \sim 1$, $q^{-1} \sim 10^{4}$ kms) invoked for ducting the radiowaves through the corona, then we have shown that they are relatively ineffective in scattering (diffusing) unstable Langmuir waves into stable regions of k-space. In this case, one may turn to nonlinear and/or quasilinear processes for an explanation of the saturation mechanism.

Acknowledgements

We acknowledge conversations with R. Lin, C. Harvey, C. Lacombe, G. Dulk and J.L. Steinberg. One of us (LM) wishes to thank L. Celnikier and A. Mangeney for interesting discussions. This work was supported by the Air Force Office of Scientific Research (Grant No. 84-0007), the National Aeronautics and Space Administration (Grant No. NAGW-91), and by the National Science Foundation, Atmospheric Sciences Section (Grant No. ATM-8020426), to the University of Colorado.

References

Bougeret, J.L., and Steinberg, J.L.: 1977, Astron. Astrophys. 61, 777.

Celnikier, L.M., Harvey, C.C., Jegon, R., Kemp, M., and Moricet, P.: 1983, Astron. Astrophys. 126, 293.

Cronyn, W.M.: 1972, Astrophys. J. 171, L101.

Duncan, R.A.: 1979, Solar Phys. 63, 389.

Goldman, M.V., and DuBois, D.F.: 1982, Phys. Fluids. 25, 1062.

Grognard. R.J.-M.: 1982, Solar Phys. 81, 173.

Gurnett, D.A., Marsch, E., Philipp, W., Schwenn, R., and Rosenbauer, H.: 1979, J. Geophys. Res., 84, 2029.

Lin, R.P., Potter, D.W., Gurnett, D.A., and Scarf, F.L.: 1981, Astrophys. J. 251, 369.

Nishikawa, K., and Ryutov, D.D.: 1976, J. Phys. Soc. Japan 41, 1757.

Robinson, R.D.: 1983, Proc. Astron. Soc. Australia 5, 208.

Smith, D.F., and Sime, D.: 1979, Astrophys. J. 233, 998.

Weatherall, J., Nicholson, D.R., and Goldman, M.V.: 1981, Astrophys. J. 246, 306.

Appendix: Evaluation of Φ, P_{in}, P_{out} with a model of spectrum

a) Flux of energy

Substituting the ansatz (23) into Equation (21) one obtains

$$\Phi = 2\pi/\sqrt{e}\, D_o\, (v_b v_e)^3\, (1+x_o)\, x_o^3\, \Delta W. \tag{A1}$$

b) Input/Output of power P_{in}, P_{out}

In order to simplify the integrals in Equations (18)-(19) we replace the Maxwellian shape of the spectrum by a box with the same area:

$$W(x) = \begin{cases} W_m + 0.85\, \Delta W & \text{for } x>x_o \\ W_m & \text{for } x<x_o \end{cases} \tag{A2}$$

The integrals are then straightforward,

$$P_{in} = \sigma^+ + \sqrt{2}\pi^{3/2}\, n_b\, \omega_{pe}^3/(k^2 \Delta v v_b)\, \left\{ 1-\exp\left[-v_b^2/2\Delta v^2 (1-x_o)^2 \right] \right\}\, (W_m+0.85\Delta W)$$
$$P_{out} = -\sigma^- + \sqrt{2}\pi^{3/2}\, n_b\, \omega_{pe}^3/(k^2 \Delta v v_b)\, \left\{ 1-\exp\left[-v_b^2/2\Delta v^2 (1+x_o)^2 \right] \right\}\, W_m. \tag{A3}$$

Using these expressions, the condition (20) may be rewritten in the limit $v_b/\Delta v \gg 1$, $x_o > 0$,

$$(1+0.85\, \Delta W/W_m \left\{ 1-\exp\left[-v_b^2/2\Delta v^2\, (1-x_o)^2 \right] \right\}$$
$$= 1 - (\sigma^+ + \sigma^-)\, k^2 \Delta v v_b/(\sqrt{2}\pi^{3/2}\, \omega_{pe}^3 n_b).$$

Hence the inequality (24) where the equality is reached when the spontaneous emission terms become negligible. The other inequality (25) may be

obtained in the same way by using Equations (A1) and (A3).

Figure Captions

Fig. 1 Langmuir spectrum when the diffusion is sufficiently strong to quench the beam instability by diffusing the waves out of the unstable regions of phase space into stable ones, yet not strong enough to prevent a pronounced peaking of the spectrum in the energy source area.

a) Contours of W_k (unit T_e) in the k-θ plane; the Langmuir energy piles up in the forward propagating damped modes ($\theta<\pi/2$) which are in Cerenkov resonance with the positive slope of the beam and diffuses into the backward damped propagating modes ($\theta>\pi/2$).

b) $W_k(\theta)$ in unit of T_e at $kv_b/\omega_{pe} = 1.62$; note the substantial angular gradient for $\theta\approx\pi/4$.

The parameters used are: $n_b = 5\cdot10^{-7}$, $v_b = 90\ v_e$, $\Delta v = 20\ v_e$, $n_T(v_T/v_e)^5 = 20$, and isotropic density fluctuations with $\delta n/n = 5\cdot10^{-4}$.

Fig. 2 Marginal stability boundary of the beam growth rate Γ_{crit} as a function of $kv_b/\omega_{pe} = x_o^{-1}$ (cf. Equation (28)). If, at a given kv_b/ω_{pe}, the growth rate of the Langmuir waves maximised over the angle θ, $\gamma_{max}^{(b)} = 0.38\ n_b/(k\Delta v)^2$, is smaller than $\Gamma_{crit}\ (kv_b/\omega_{pe})$, the instability at that wavenumber is quenched. In the plot shown, the density fluctuations are chosen isotropic with $\delta n/n = 5\cdot10^{-4}$ and the electron distribution function consists of a Maxwellian background without tail and of a beam with varying parameters (solid line: $v_b = 90\ v_e$, $\Delta v = 20\ v_e$; white circles: $v_b = 90\ v_e$, $\Delta v = 30\ v_e$; crosses: $v_b = 60\ v_e$, $\Delta v = 20\ v_e$).

The rapid fall-off of Γ_{crit} is contrasted with the slow k^{-2} decrease of $\gamma_{max}^{(b)}$ indicated in dashed line for a beam of $n_b = 5 \cdot 10^{-7}$, $v_b = 90\ v_e$. $\Delta v = 20\ v_e$. Thus, due to the diffusion, waves with the fastest growth rate may be stable while waves with bigger wavenumbers and slower growth rate are unstable.

Fig. 3 Marginal stability boundary Γ_{crit} as in Figure 2 except that a nonthermal tail in the electron distribution is considered. The parameters of the tail have been fitted from the nonthermal component observed by Lin et al., 1981, $n_T(v_T/v_e)^5 = 20$. In that situation, a beam of parameters $n_b = 5 \cdot 10^{-7}$, $v_b/v_e = 90$, $\Delta v/v_e = 20$, is completely stabilized (cf. $\gamma_{max}^{(b)}$ in dashed line). Yet, were the beam 40% more dense, $n_b = 7 \cdot 10^{-7}$, a small range of $k\lambda_D$ would be unstable (dotted line).

Fig. 4 Γ_{crit} for various parameters. The marginal stability boundary Γ_{crit} of Figure 3 is indicated in the dashed-line for comparison purposes.

a) $v_b = 90\ v_e$, $\Delta v = 20\ v_e$. $n_T(v_T/v_e)^5 = 20$, $\delta n/n = 1.5\ 10^{-3}$

b) same as for a) except $v_b = 60\ v_e$

c) same as for a) except $n_T(v_T/v_e)^5 = 2$.

Fig. 5 A simple model of anisotropic density fluctuations. The function $\tilde{C}(\theta)$ (cf. Equation (6)) is assumed to be at two levels.

Fig. 6 Spectrum of density fluctuations a) and corresponding spectrum of Langmuir waves b). On panel a) the equilines of Log $(q^2\ (\delta n/n)^2|_q)$ are plotted in the q-θ plane. The density fluctuations are assumed

to be strong and highly peaked in the plane perpendicular to the beam or magnetic field axis (cf. Equation (19) with $a = 7 \cdot 10^{-4}$). On panel b) the equilines of Langmuir energy are plotted in the k-θ plane for the "nominal" beam-tail parameters ($n_b = 10^{-6}$, $v_b = 90\ v_e$, $\Delta v = 20\ v_e$, $n_T(v_T/v_e)^5 = 20$). Note the substantial concentration of energy in the forward propagating modes.

Table for Detailed Balance

"nominal" parameters
for the beam and the tail

$n_b = 10^{-6}$ $\quad \Delta v = 20\ v_e$ $\quad v_b = 90\ v_e$ $\quad n_T v_T^5 = 20\ v_e^5$

$k\lambda_D$	$\gamma_{max}^{(b)}/\omega_{pe}$	$\gamma^{(T)}/\omega_{pe}$	$\bar{\gamma}^{(b)}/\omega_{pe}$	$\bar{S}^{(b)}/T_e\omega_{pe}$	$S^{(T)}/T_e\omega_{pe}$	W_k/T_e
$1.11\ 10^{-2}$	0	$-1.3\ 10^{-8}$	$-1.4\ 10^{-6}$	$6.4\ 10^{-3}$	$3.5\ 10^{-5}$	$2.2\ 10^{3}$
$1.3\ 10^{-2}$		$-2.9\ 10^{-8}$	$-8.3\ 10^{-7}$	$5.9\ 10^{-3}$	$5.7\ 10^{-5}$	$3.4\ 10^{3}$
$1.5\ 10^{-2}$	$3.9\ 10^{-6}$	$-6.0\ 10^{-8}$	$-3.9\ 10^{-7}$	$4.5\ 10^{-3}$	$8.9\ 10^{-5}$	$5.1\ 10^{3}$
$1.7\ 10^{-2}$	$3.0\ 10^{-6}$	$-1.1\ 10^{-7}$	$-1.8\ 10^{-7}$	$3.3\ 10^{-3}$	$1.3\ 10^{-4}$	$6.0\ 10^{3}$
$1.9\ 10^{-2}$	$2.4\ 10^{-6}$	$-1.9\ 10^{-7}$	$-8.4\ 10^{-8}$	$2.5\ 10^{-3}$	$1.8\ 10^{-4}$	$4.7\ 10^{3}$
$2.2\ 10^{-2}$	$1.8\ 10^{-6}$	$-4.1\ 10^{-7}$	$-3.0\ 10^{-8}$	$1.6\ 10^{-3}$	$2.8\ 10^{-4}$	$2.2\ 10^{3}$
$2.5\ 10^{-2}$	$1.4\ 10^{-6}$	$-7.7\ 10^{-7}$	$-1.2\ 10^{-8}$	$1.1\ 10^{-3}$	$4.1\ 10^{-4}$	970
$3.0\ 10^{-2}$	$9.8\ 10^{-7}$	$-1.9\ 10^{-6}$	$-3.5\ 10^{-9}$	$6.4\ 10^{-4}$	$7.0\ 10^{-4}$	350
$3.5\ 10^{-2}$	$7.3\ 10^{-7}$	$-4.1\ 10^{-6}$	$-1.3\ 10^{-9}$	$4.1\ 10^{-4}$	$1.1\ 10^{-3}$	185
$4.0\ 10^{-2}$	$5.6\ 10^{-7}$	$-8.0\ 10^{-6}$	$-5.5\ 10^{-10}$	$1.7\ 10^{-3}$	$2.7\ 10^{-3}$	121
$6.0\ 10^{-2}$	$2.5\ 10^{-7}$	$-6.1\ 10^{-5}$	$-5.8\ 10^{-11}$	$8.1\ 10^{-5}$	$5.6\ 10^{-3}$	47
$8.0\ 10^{-2}$	$1.4\ 10^{-7}$	$-2.6\ 10^{-4}$	$-1.5\ 10^{-11}$	$3.4\ 10^{-5}$	$1.4\ 10^{-2}$	26
$1.0\ 10^{-1}$	$9.1\ 10^{-8}$	$-7.9\ 10^{-4}$	$-5.8\ 10^{-12}$	$1.7\ 10^{-5}$	$2.6\ 10^{-2}$	17

RUNNING HEAD: Quenching of the Beam-Plasma Instability by Density Fluctuations

MAILING ADDRESS: L. Muschietti
Department of Astrophyical, Planetary & Atmospheric Sciences
University of Colorado
Campus Box 391
Boulder, CO 80309 USA

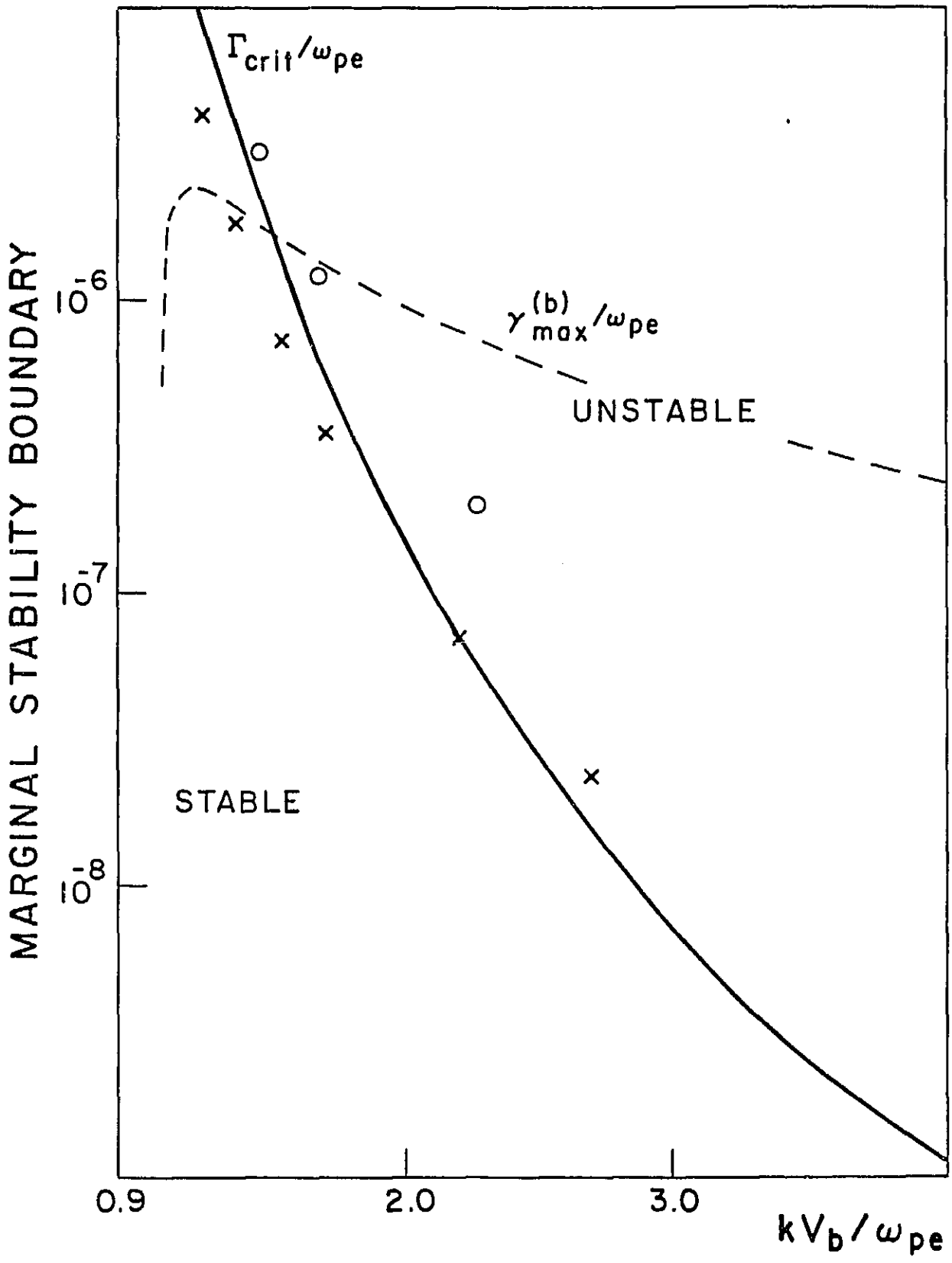
MARGINAL STABILITY BOUNDARY
10^{-6}
10^{-7}
10^{-8}
$\Gamma_{crit}/\omega_{pe}$
$\gamma^{(b)}_{max}/\omega_{pe}$
UNSTABLE
STABLE
0.9
2.0
3.0
kV_b/ω_{pe}

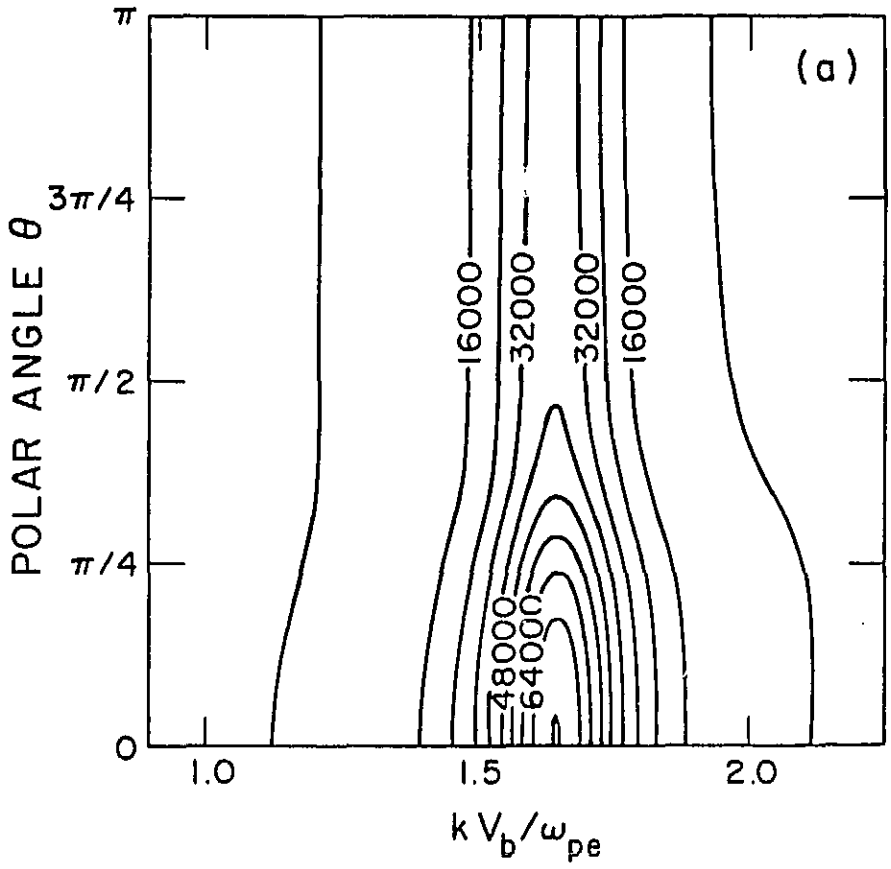
(a)
POLAR ANGLE θ
π
3π/4
π/2
π/4
0
16000
32000
32000
16000
48000
64000
1.0
1.5
2.0
k V_b/ω_pe

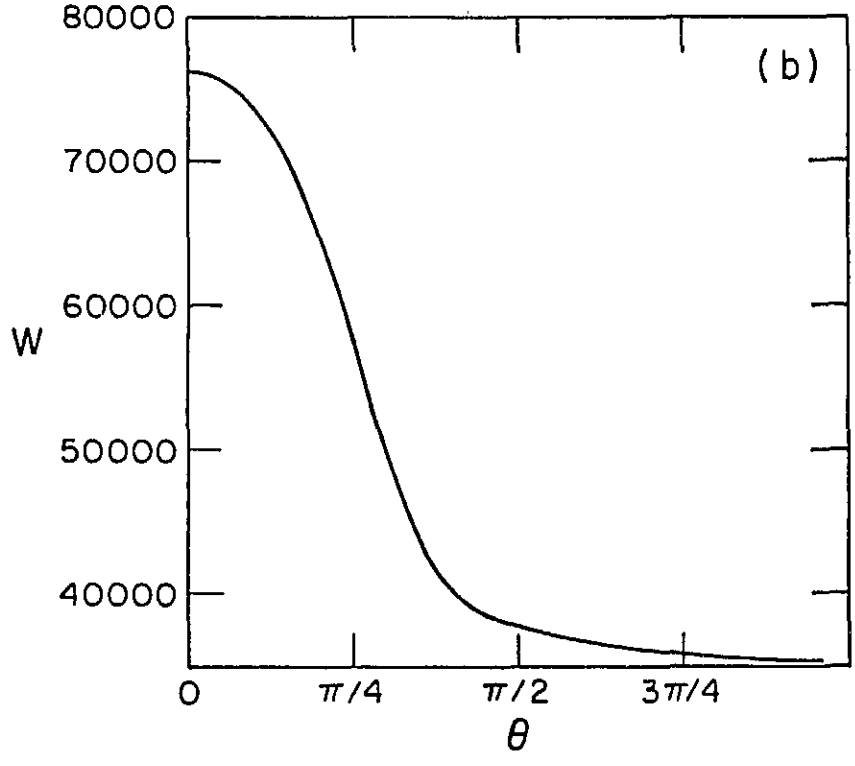
(b)
W
80000
70000
60000
50000
40000
0
π/4
π/2
3π/4
θ

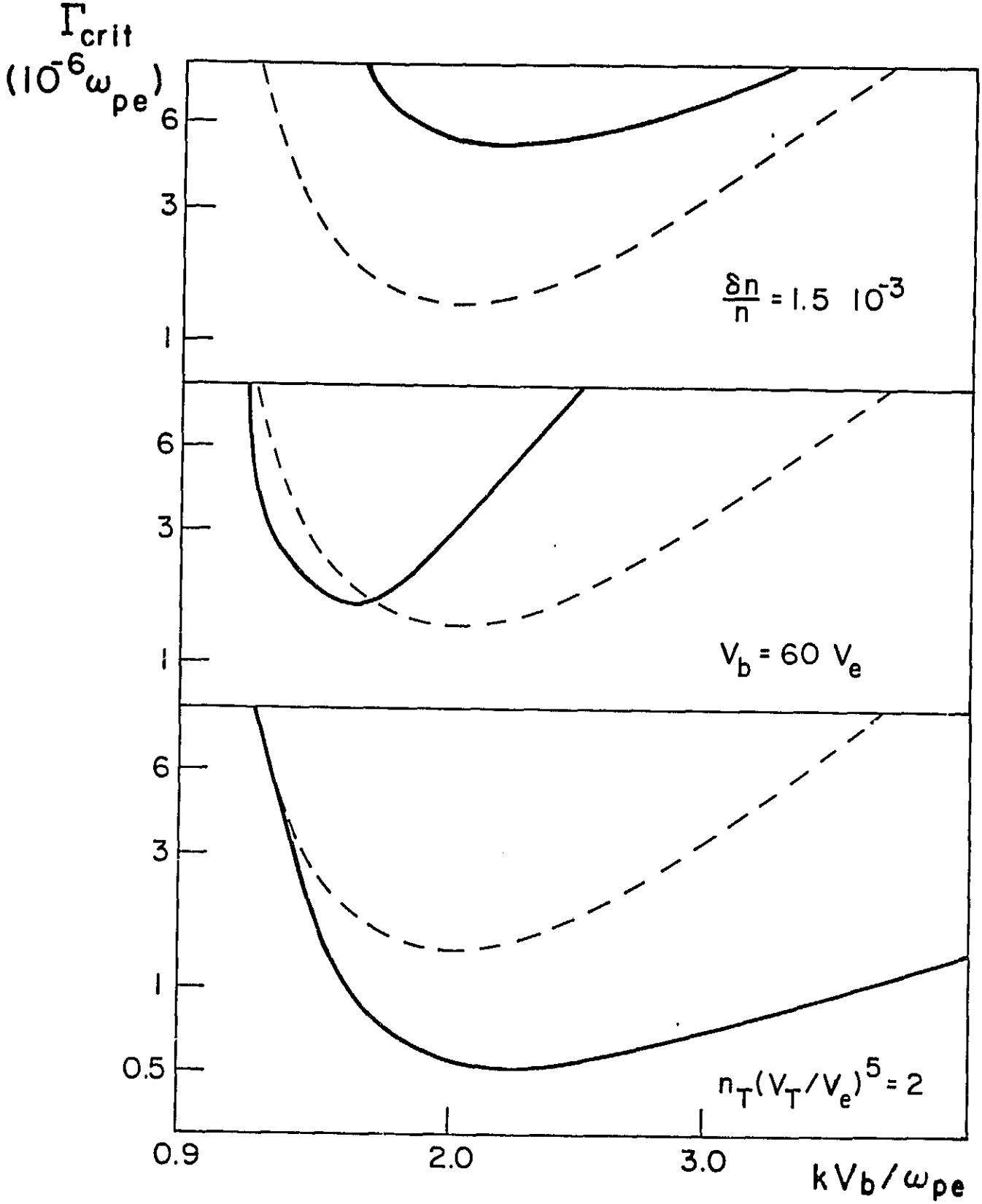
Γ_{crit}
$(10^{-6}\omega_{pe})$
6
3
1
$\frac{\delta n}{n} = 1.5\ 10^{-3}$
6
3
1
$V_b = 60\ V_e$
6
3
1
0.5
$n_T(V_T/V_e)^5 = 2$
0.9
2.0
3.0
kV_b/ω_{pe}

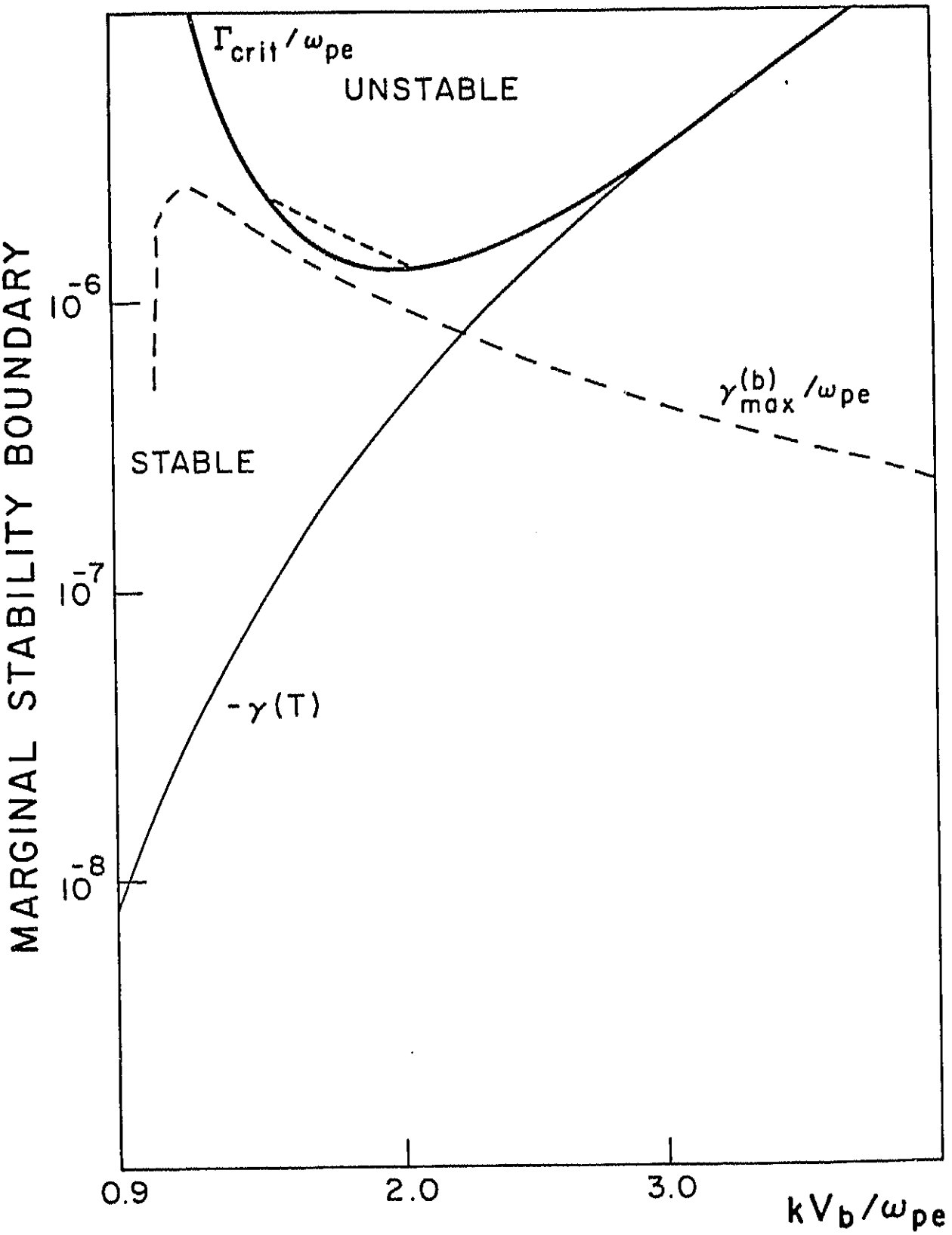
MARGINAL STABILITY BOUNDARY
$\Gamma_{crit}/\omega_{pe}$
UNSTABLE
STABLE
$\gamma^{(b)}_{max}/\omega_{pe}$
$-\gamma(T)$
10^{-6}
10^{-7}
10^{-8}
0.9
2.0
3.0
kV_b/ω_{pe}

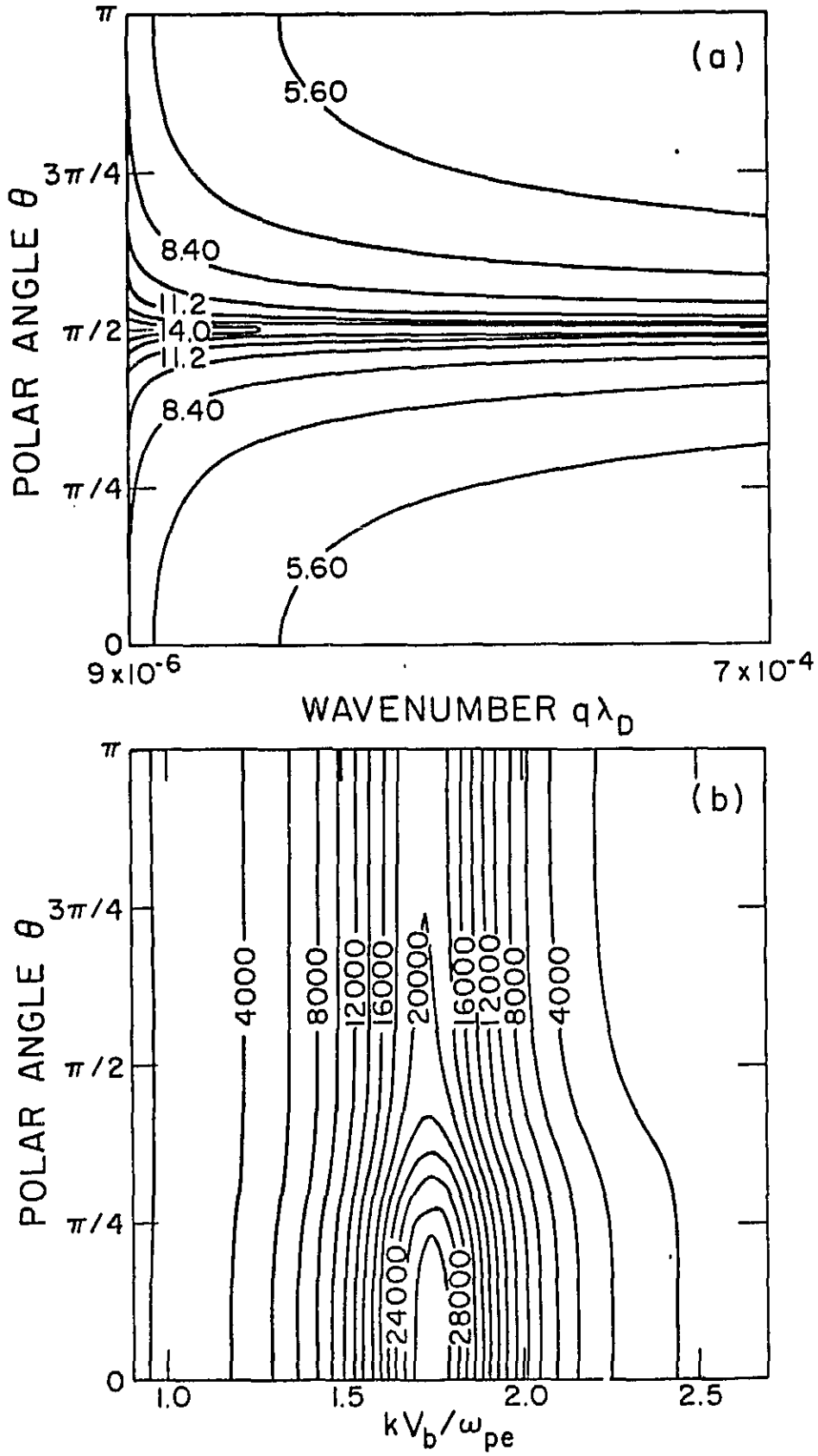
(a)
5.60
8.40
11.2
4.0
11.2
8.40
5.60
π
3π/4
π/2
π/4
0
POLAR ANGLE θ
9x10⁻⁶
7x10⁻⁴
WAVENUMBER qλD
(b)
4000
8000
12000
16000
20000
16000
12000
8000
4000
24000
28000
1.0
1.5
2.0
2.5
kVb/ωpe

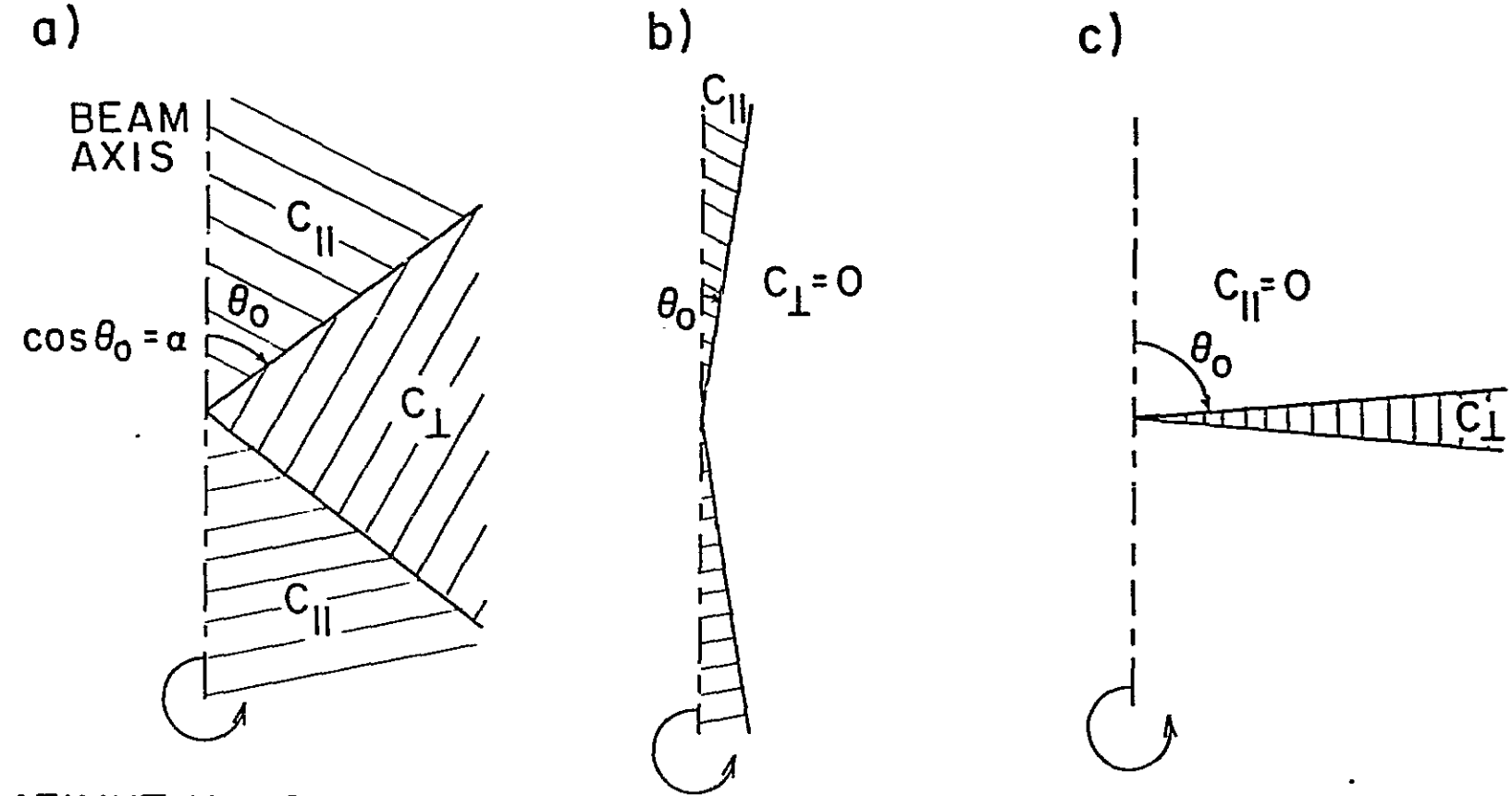

AZIMUTHAL SYMMETRY

MULTIPLE RAMAN UP-CONVERSION OF RADIATION FROM PRE-EXISTING LANGMUIR TURBULENCE

D. Russell, M. Goldman, and D. Newman

September 1984

Abstract

We consider the equilibrium states described by a damped and driven kinetic equation governing the evolution of the spectrum of radiation in a stationary Langmuir-turbulent plasma. Both Langmuir and transverse spectra are assumed to be one-dimensional in wave-number space. A source of radiation at the plasma frequency and a uniform rate of dissipation at the higher harmonics are assumed. The radiation is characterized by an effective temperature, z, proportional to the Langmuir energy density and inversely proportional to the dissipation rate of the transverse waves. If $z < 1$ the equilibrium photon spectrum decreases with increasing frequency as a power law in z. If $z > 1$, photons scattered out of certain regions of phase space may return at a significnat rate, and the spectrum is found to have a global maximum above the plasma frequency, ω_p. The location of this maximum is proportional to $z^{1/3}\ \omega_p$, which may be many times the plasma frequency. Applications to a laser-plasma experiment and to the solar-wind environment are discussed.

I. Introduction and Model Kinetic Equation

Although there a number of important applications, little is known about mechanisms for producing radiation at frequencies much higher than the maximum plasma frequency in non-magnetic plasmas. Radiation at high multiples of the plasma frequency has been observed in laser-pellet experiments,[1] in relativistic beam-plasma interactions,[2] and in low-energy beam-plasma interactions.[3,4] It is also thought to play a role in astrophysical phenomena.[5]

In relativistic beam-plasma systems, it has been suggested[2] that the high energy of beam electrons could be tapped by Compton-conversion of a beam-electron and a plasma wave into a high-energy photon together with a lower-energy electron.[6] Recent work shows that the growth-rate for this process is very low for a wide variety of Langmuir spectra.[7]

Radiation at twice the plasma frequency can be produced by coalescence of two Langmuir waves, and the process appears to be well-documented by examples of radio-wave emissions from the solar corona.[8] However, the emissivity is proportional to the square of the intensity of the Langmuir-wave spectrum, and the process is therefore not very efficient unless the Langmuir turbulence is quite intense (Langmuir energy-density on the order of the particle energy-density). Emission at the n-th harmonic of the plasma frequency by n-plasmon coalescence is proportional to the n-th power of the Langmuir wave intensity, so that this process would be still less efficient at weak levels of Langmuir turbulence.

Another alternative is to begin with radiation near the plasma frequency or its second harmonic, produced by instability or by external sources, and to allow it to Raman-scatter repeatedly from pre-existing Langmuir turbulence. At each step such scattering will produce frequency upshifts (anti-Stokes process) and downshifts (Stokes process--which is permissible as long as the shift does not go below the plasma frequency). The resulting radiation spectrum may exhibit frequency components significantly above the plasma frequency.

This is the process we shall consider in this paper. For sufficiently weak photon damping rates, we find that multiple Raman scatter to the n-th harmonic is not proportional to the n-th harmonic of the Langmuir intensity, so this process can be more efficient than the multiple plasmon coalescence mechanism under certain conditions.

The multiple Raman scatter process works best in a hot plasma, with the radiation in contact with the turbulence for a sufficiently long time. This could be expedited in various ways: In astrophysical applications the spatial extent of the turbulence may be considerable. In laboratory plasmas there may be multiple reflections from chamber walls.

Consider the scattering interactions of two species of waves illustrated in Figure 1. In a plasma, for example, the waves labeled by k could be transverse waves scattering off ion acoustic waves labeled by q. This process is commonly called Brillouin scattering. If, instead, the waves labeled by q are Langmuir waves then the scattering is termed Raman. In addition to higher-order wave-wave interactions not depicted in Figure 1, Brillouin and

Raman scattering generally compete in determining the evolution of a transverse spectrum. (Wave-particle interactions are ignored in this paper.) We assume the presence of an enhanced background of Langmuir turbulence, (rather than ion acoustic turbulence), and focus our attention on the effect such turbulence has on the evolution of an externally produced electromagnetic (transverse) spectrum.

We take the Langmuir waves to be statistically stationary: If $W^L(\underline{k})$ denotes the ensemble-averaged energy density of Langmuir waves at wave-vector $\underline{k}$ then $W^L(\underline{k})$ is assumed not to change in time. For example, the Langmuir waves may be maintained in steady state by a source such as an electron beam. In any case, we ignore the back-reaction of the transverse spectrum on the Langmuir spectrum. We are justified in doing so provided the transverse spectrum is far less energetic than the Langmuir spectrum responsible for the scattering. To summarize, we are considering a plasma in which the ion-acoustic, transverse, and Langmuir wave energy densities are ordered as follows.

$$W^{ia} \ll W^T \ll W^L$$

We also rely on the second inequality to justify our neglect of the stimulated scattering of transverse waves in Sections II and III. This process is described by terms in the kinetic equation that are proportional to $(W^T)^2$, whereas the terms that we retain in the equation are proportional to $W^L W^T$. In general, if stimulated scattering must be included in the evolution of the transverse spectrum then so must the evolution of the Langmuir wave spectrum, since in this case $W^T \sim W^L$. (We briefly describe equilibrium and temporal evolution in the presence of stimulated scattering in Secs. IV and V.)

The scattering that we consider here is resonant, that is,

$$k = k' \pm q \tag{2a}$$

and

$$\omega(k) = \omega(k') \pm \omega_p \tag{2b}$$

are enforced in the kinetic equation (see Fig. 1). Here ω_p denotes the plasma frequency and we neglect the thermal dispersion of Langmuir waves.

Our final assumption is that the Langmuir spectrum is confined to only one direction in $\underline{q}$-space, i.e., that it is maintained by a narrow source. With our source of radiation taken to be in this same direction, the kinetic equation describes transverse-wave evolution in a one-dimensional k-space and therefore ignores effects such as angular diffusion.

From the dispersion relation for transverse waves

$$\omega(k)^2 = \omega_p^2 + c^2k^2$$

and using Eq. (2a) and Eq. (2b) it is easily seen that only Langmuir waves with wave numbers in the interval

$$\frac{\omega_p}{c} \leq q \leq \sqrt{3}\,\frac{\omega_p}{c}$$

contribute to the scattering. We ignore any variation of $W^L(q)$ on this interval (see Fig. 2), and simply assume a flat spectrum.

According to Equation (2b), only transverse waves whose frequencies differ by a multiple of the plasma frequency will interact with one another. Therefore with a source of radiation at the plasma frequency, the transverse spectrum (i.e., the ensemble-averaged energy density) will evolve only at the harmonics of ω_p. Let n be the harmonic number,

$$n \equiv \omega(k)/\omega_p .$$

Then the usual "Golden Rule" kinetic equation[9] describing this scattering may be written in the following form. (We outline a derivation of this equation in Appendix A.)

$$\begin{aligned}\frac{dU_n}{dt} = & -W\,(A_n^3 + B_n^3)\,U_n/n \\ & + W\,(A_n^3\, n/(n+1)^2\, U_{n+1} + B_n^3\, n/(n-1)^2\, U_{n-1}) \\ & + V\,(U_n/n)\,(A_n^2\, U_{n+1}/(n+1)^2 - B_n^2\, U_{n-1}/(n-1)^2) \\ & - 2\,\gamma_n\, U_n + S_n \end{aligned} \qquad (3a)$$

Here, U_n is the transverse-wave energy density at the n-th harmonic normalized to the ambient thermal energy density of the electrons, $4\pi n_o T_e$ (n_o is the average plasma density, and T_e is the electron temperature), and time is measured in units of the plasma frequency, ω_p. The coefficient W is proportional to the Langmuir energy density, and is defined as

$$W \equiv \frac{1}{8\pi}\,(v_e/c)^2\,\alpha\,W^L , \qquad (3b)$$

where v_e is the thermal velocity of the electrons; c is the speed of light in a vacuum; W^L is the total energy density of Langmuir waves normalized to $4\pi n_o T_e$; and α is a numerical reduction factor that selects, from a more general Langmuir spectrum, that portion of the spectrum which is contained in q-space between ω_p/c and $\sqrt{3}\omega_p/c$ and therefore active in the scattering considered here:

$$\alpha \leq 0.7.$$

Equality holds if all of the Langmuir energy is contained between ω_p/c and $\sqrt{3}\omega_p/c$ (see Fig. 2).

The scattering coefficients are defined as follows.[9] (See Appendix A.)

$$A_n \equiv \sqrt{[(n+1)^2 - 1]} - \sqrt{(n^2-1)} \tag{3c}$$

$$B_n = \begin{cases} A_{n-1} & , \quad n \geq 2 \\ 0 & , \quad n = 1 \end{cases} \tag{3d}$$

Equation (3d) expresses the result of detailed balancing. Using it one can easily show that in the absence of sources and dissipation ($\nu_n = S_n = 0$) the total energy density, $\sum U_n$, is conserved.

The coefficient of the terms which describe stimulated scattering is

$$V \equiv \frac{1}{8\pi} (v_e/c)^2 .$$

Therefore, roughly speaking, the ratio of the stimulated to the linear scattering rate ($\sim$WU) is

$$\alpha \sim VU/W \quad .$$

When this ratio is much less than one, the stimulated scattering is ignorable, and the evolution of the spectrum is linear in U.

For simplicity, we assume a source term for radiation at the fundamental only,

$$S_n = S\ \delta_{1,n} \quad .$$

Throughout this paper we take the source at ω_p only, but it is straightforward to generalize our results to include different source configurations.

An independent source of radiation at $2\omega_p$ (n=2) is the coalescence of two Langmuir waves into a transverse wave. An important question is whether or not the coalescence process produces a stronger source of radiation at $2\omega_p$ than does Raman scattering of a given source at ω_p into that second harmonic. In fact, multiple Langmuir wave coalescence into radiation at the nth harmonic of the plasma frequency generally should be compared to the nth-order radiation produced by multiple Raman scattering. However, in the one-dimensional k-space we are assuming the matrix elements for coalescence vanish so that this process is absent. (See Ref. 9 pg. 354, for example.)

We take all harmonics to be dissipated at a constant rate, γ_d:

$$\gamma_n = \gamma_d \quad , \quad n = 2,3, \ldots \tag{4a}$$

Loss of energy at $n\omega_p$ by convection out of a bounded plasma occurs at a rate equal to the group velocity at $n\omega_p$ divided by the size of the plasma, so the dimensionless radiation dissipation rate is taken to be:

$$\gamma_d = \frac{c}{\omega_p R} \tag{4b}$$

where R is the characteristic length of the plasma. We have approximated the group velocity by the speed of light, c (appropriate for the higher harmonics); and, again, all rates are measured in units of the plasma frequency.

With this scenario of injection at the fundamental, Equations (3) predict a cascade of energy up to higher harmonics via Raman scattering. Our primary concern in this paper is with the equilibrium spectra that result from this cascade. Clearly such equilibria must exist if the damping rate at the fundamental, γ_1, is positive (incoherent source of fundamental radiation); in this case all harmonics are dissipated exponentially fast, whereas the injection of energy at the source proceeds only linearly with time. If the damping rate at the fundamental is assigned a negative value, to simulate a linear instability at ω_p, then the cascade either culminates in a stationary state or else the energy in the spectrum diverges with increasing time. In Sections II through IV we assume that a stationary state is eventually reached by the solution of Equation (3a) for the particular choice of γ_1. In Section II we restrict our attention to equilibria for which

$$\alpha W^L >> U_n, \; n = 1,2,\ldots$$

so that the linearized kinetic equation (i.e., Eq. (3a) without the stimulated scattering terms proportional to V) adequately decribes the stationary state. Under this assumption it is possible to find analytic approximations to the equilibria using a continued-fraction representation. That analysis is carried out in Section III. In Section IV we present examples of equilibrium spectra, including a case in which the nonlinear terms (stimulated scattering) are not ignored. Unbounded behavior is considered in Section V. Concluding remarks appear in Section VI.

II. Equilibrium Spectra

With $\partial_t U_n$ set equal to zero for all n in the linearized verison of Equation (3a), we are faced with the task of solving an inhomogeneous system of linear, algebraic equations. The number of these equations is, in principle, infinite, although we expect the spectrum to fall off rapidly at sufficiently large n to permit a truncation. Rather than impose an a priori truncation, we proceed, instead, to solve the equations recursively, writing each U_n as a product of unending continued fractions. This will yield the exact solution for all n. With one very good approximation to the scattering coefficients, the continued fractions are summable in terms of Bessel functions (cf. Sec. III). This method is applicable to other discrete systems enjoying linear nearest-neighbor interactions, although summability depends crucially on the form of the coefficients.

For sufficiently weak photon dissipation rates, certain solutions we obtain clearly demonstrate scattering to high harmonics of ω_p with efficiencies well above unity (see Fig. 3). This is contrary to the popular belief that the spectrum should in any case fall off as $(W^L)^n$. The reasoning which leads to that conclusion ignores the scattering back down to lower frequencies described by the "A" coefficients in Eq. (3a). The scattering down results in an accumulation or "bottle-necking" of transverse energy at intermediate frequencies that is responsible for the observed extremum in the spectrum that we will approximate analytically in Sec. III.

For convenience, we introduce

$$F_n \equiv U_n/n^2 \tag{5}$$

and write the stationary, linearized version of Equation (3a) in the following form. (We suppress the exponents on the scattering coefficients.)

$$[2n\gamma_n + WA_n + WB_n]\, F_n - WA_n\, F_{n+1} - WB_n F_{n-1} = S\, \delta_{1,n} \tag{6}$$

For illustrative purposes, we truncate the system to only the fundamental, F_1, and its first harmonic, F_2. Then we can easily solve Equation (6):

$$F_1 = S \cdot \cfrac{1}{2\gamma_1 + WA_1 + \cfrac{1}{- \cfrac{(4\gamma_2 + WA_1 + WA_2)}{W^2 A_1^2}}}$$

and

$$F_2 = F_1 \cdot \cfrac{1}{\cfrac{4\gamma_2 + WA_1 + WA_2}{WA_1}}$$

Retaining three modes, the solution is:

$$F_1 = S \cdot \cfrac{1}{2\gamma_1+WA_1 + \cfrac{1}{-\cfrac{(4\gamma_2+WA_1+WA_2)}{WA_2} + \cfrac{1}{\cfrac{(6\gamma_3+WA_2+WA_3)}{A_2^2/A_1^2}}}}$$

$$F_2 = F_1 \cdot \cfrac{1}{\cfrac{4\gamma_2+WA_1+WA_2}{WA_1} + \cfrac{1}{-\cfrac{(6\gamma_3+WA_2+WA_3)}{WA_2^2/A_1}}}$$

and

$$F_3 = F_2 \cdot \cfrac{1}{\cfrac{6\gamma_3+WA_2+WA_3}{WA_2}} \qquad (7)$$

As we increase the number of modes retained in the truncation, the following pattern emerges.

Let $\hat{f}_\ell$ be the continued fraction,

$$\hat{f}_\ell \equiv \cfrac{1}{f_{\ell 1} + \cfrac{1}{f_{\ell 2} + \cfrac{1}{f_{\ell 3} + \cfrac{1}{f_{\ell 4} + \ldots}}}} \qquad (8a)$$

with elements defined by

$$f_{\ell\, j} \equiv \frac{2(\ell+j)\nu_{\ell+j}+WA_{\ell+j}+WA_{\ell+j-1}}{g_{\ell\, j}} \quad , (A_0 \equiv 0) \tag{8b}$$

and

$$g_{\ell\, j} \equiv \begin{cases} -W^2A^2_{\ell+j-1}/g_{\ell\, j-1} & j>1 \\ WA_\ell & \ell>0,\ j=1 \\ 1 & \ell=0,\ j=1 \end{cases} . \tag{8c}$$

Then

$$F_{k+1} = S\prod_{\ell=0}^{k} \hat{f}_\ell \quad . \tag{9}$$

Equations (8 and 9) are the exact solution of Eq.(6) and give us, using Eq. (5), the exact stationary states of the linearized kinetic equation. Writing the solution in this form is particularly useful because of the slow variation of A_n with n for $n \geq 3$. (Notice from Eq. (3c) that A_n is approximatly equal to one if $n \geq 3$.) We were careful to factor this slow dependence out of the scattering terms in the kinetic equation for the following reason.

With our assumption that the ν_n's are constant ($= \nu_d$) for $n \geq 2$ and the approximation of the A_n's by unity for all n, we can find simple closed-form expressions for all F_n with $n \geq 2$ in terms of F_1. Therefore, we will have approximations to all U_n/U_1, c.f. eq. (5), and, hence, to the efficiency of the net up-scattering in the stationary state. Notice from Eqs.

(8 and 9) that we do not need to specify γ_1 or S in order to determine this efficiency. These parameters serve only to determine the overall size or total energy density of the spectrum and do not effect its shape. Of course we assume that the particular choice of γ_1 leads to a stationary spectrum, although for sufficiently large, negative values of γ_1 the behavior is unbounded in time. See Section V.

III. Analytic Approximations

With all A_n's approximated by unity and, for the case of a constant dissipation rate at the higher harmonics,

$$A_n = 1 \qquad n \geq 1$$
$$\gamma_n = \gamma_d \qquad n \geq 2 \quad ,$$

we find from Eqs. (8a thru c) that the continued fractions have the following simple form if $\ell \geq 1$.

$$\hat{f}_\ell = \cfrac{1}{\frac{2(\ell+1+z)}{z} - \cfrac{1}{\frac{2(\ell+2+z)}{z} - \cfrac{1}{\frac{2(\ell+3+z)}{z} - \ldots,}}} \qquad (\ell \geq 1) \tag{10}$$

with

$$z = W/\gamma_d \quad .$$

This continued fraction is summable as a ratio of Bessel functions,[10]

$$\hat{f}_\ell = J_{z+\ell+1}(z)/J_{z+\ell}(z) \quad , \tag{11}$$

where $J_\nu(z)$ denotes the Bessel function of the first kind of order ν.[11] It follows from Eq. (9) that

$$F_n = F_1 \, J_{z+n}(z)/J_{z+1}(z) \quad , \tag{12}$$

and thus from Eq. (5) that

$$U_n = U_1 \cdot n^2 \cdot J_{z+n}(z)/J_{z+1}(z) \quad . \tag{13}$$

Notice the recursion relation implied by, and implying, Eq. (10):

$$\hat{f}_\ell = 2(\ell+z)/z \quad - \quad 1/\hat{f}_{\ell-1} \tag{14}$$

If we multiply this equation through by F_ℓ and use Eq. (9) we discover that

$$F_{\ell+1} + F_{\ell-1} = \frac{2(\ell+z)}{z} F_\ell \quad .$$

This familiar three-term recursion relation is just Eq. (6) (n>1) and is satisfied by $F_\ell(z) = J_{\ell+z}(z)$, among a great many other choices.[11] However, the continued fraction expansion, Eq. (10), specifies F_ℓ exactly as Eq. (12).

Using simple properties of the Bessel functions it is easy to see that

$$0 < J_{z+n}(z)/J_{z+1}(z) < 1 \text{ if } z > 0.$$

Therefore, Eq. (13) makes sense (i.e., U_n is positive for all n) provided only that U_1 is positive. Requiring U_1 to be positive, in the presence of a linear instability at the fundamental ($\nu_1 < 0$) enables us to locate the threshold for saturating the instability using our exact expression for F_1, Eqs. (8 and 9). We have observed that negative values of F_1 imply that the numerical solution of the kinetic equation is not bounded in time. We discuss unbounded behavior in Sec. V.

We will assume that U_1 is positive and consider some physically interesting limiting forms of our expression for the equilibrium radiation spectrum. The accuracy of our formula, Eq. (13), will be tested by comparing its predictions with numerical solutions of Eqs. (3).

IV. Examples

It is noteworthy that larger values of z result in more efficient up-scattering. When the scattering rate exceeds the dissipation rate at the lower harmonics ($z > 1$) significant up-scattering occurs, producing an extremum in the spectrum at a harmonic of the fundamental. When $z < 1$ no such extremum occurs, and most of the total energy resides at the fundamental.

We now consider the two limits:

A. $z \gg 1$: Strong Up-Scattering

Here we assume that most of the energy in the spectrum resides at $n \ll z$. Then using Debye's asymptotic formula for the Bessel functions[11] and retaining only leading terms in the small parameter, n/z, we obtain the following expression for the equilibrium spectrum in this case.

$$U_n \simeq U_1 n^{7/4} \exp\left[\frac{2}{3}\sqrt{\frac{2}{z}}\,(1-n^{3/2})\right] \tag{15}$$

In Fig. 3 we plot the equilibrium spectrum obtained by solving the linearized Eqs. (3) numerically, in the limit of long time, with $z = 10^3$ and $\gamma_1 = \gamma_d$. Notice that the energy densities are small enough to justify our neglect of the stimulated scattering. (Here, as in Cases B and C below, we take the dissipation to be due to convection, $\gamma_d = c/R\omega_p$, and ignore collisional damping, for example.)

Agreement between the numerical solutions and the predictions of our formula, Eq. (15), is quite good and improves at the higher harmonics. In particular, we call attention to the maximum in the spectrum at n = 12. The formula predicts a maximum at

$$n_m = (\frac{7}{4\sqrt{2}})^{2/3} z^{1/3} \quad ,$$

which is equal to 11.5 if z is 10^3.

Certain of the parameters used in Fig. 3 are characteristic of the solar corona, although it is important to note that Langmuir wave energy densities as high as those we are assuming ($\alpha W^L = 0.7$) have never been observed in the solar wind, where $\alpha W^L \leq 10^{-5}$ is the rule. Such low levels of background Langmuir turbulence will not produce the strong up-scattering illustrated in Fig. 3, in a plasma the size of the solar corona.

It may, however be worth noting that larger (hypothetical) stellar coronas could demonstrate strong up-scattering of fundamental radiation, even at weak levels of Langmuir energy density. To produce Fig. (3) with $\alpha W^L = 7 \times 10^{-6}$ we would require a corona 10^{14} metres in radius, or 10^5 times the size of the solar corona. (See the caption to Fig. (3), and recall that $z \sim \alpha W^L R$, where R is the spatial extent of the plasma.)

Similar conclusions have been reached in a study of the diffusive limit (i.e., the high frequency limit) of the kinetic equation by Colgate and his co-workers.[12] As noted by them, the discovery of a maximum in the radiation spectrum at a harmonic of the plasma frequency may have important consequences for the theory of radio emission from quasi-stellar sources.

B. $z \ll 1$: Laser-Plasma Interaction

When $z \ll 1$, we may ignore it in the order of the Bessel functions. Expanding $J_n(z)$ about $z = 0$ and keeping only leading terms in z we obtain the following power-law formula for the equilibrium spectrum in this case.

$$U_n \simeq U_1 n^2 \left(\frac{z}{2}\right)^{n-1} \frac{1}{n!} \tag{16}$$

For a physical example of this limiting form of the spectrum we consider the observations of back-scattered light in a laser-target interaction reported by Burnett and his coworkers.[13] In this case a strong source propagates through a plasma of small extent. A typical photon remains in the plasma for a relatively short time and so is not likely to be up-scattered. The result is a spectrum that is strongly peaked at the plasma frequency. A value of z equal to 10^{-1} is appropriate for their experiment, and we have taken $\nu_1 = \nu_d$.

In Fig. (4a) we plot the equilibrium spectrum obtained by solving the linearized kinetic equation numerically. In Fig. (4b) we plot the corresponding result for the full kinetic equation, including the stimulated scattering. Crosses indicate experimental results reported by Burnett et al.

Notice that efficiencies oberved in the laser experiment are greater than those predicted by either the linear or nonlinear kinetic equations at high frequencies. The scattering at these high frequencies is off Langmuir waves with wave vectors clustered about ω_p/c. Thus, enhanced levels of plasma turbulence near this wave number (i.e., that wave number excited by the laser) would account for the observed enhanced efficiencies, in the context of Raman up-scattering.

The nonlinear theory predicts smaller efficiencies than the linear theory. The effect of stimulated scattering is to suppress up-scattering and to concentrate a greater fraction of the total energy at the fundamental, ω_p, compared to the predictions of the linear theory. This result may be inferred by comparing the signs of the two nonlinear terms in the full kinetic equation (3a): radiation at n+1 causes U_n to increase with time; radiation at n-1 causes U_n to decrease with time. Thus, stimulated scattering transfers energy to low frequencies, and so supresses up-scattering.

Our numerical results are compared with the prediction of our formula for this case, Eq. (16), in Table I. Agreement with the linearized kinetic equation is excellent at the third and higher harmonics, as it should be, since our approximation to the scattering coefficients is very accurate at these harmonics.

In the experiment, the laser-source is so energetic that the stimulated scattering cannot be ignored, and this implies that the back-reaction of the Langmuir spectrum to the transverse waves ought to be considered as well, as discussed earlier. However, the stationary spectrum, obtained by integrating the nonlinear kinetic equation (3a) numerically, is reached very quickly. Starting from no radiation initially, we find that a stationary spectrum is reached within five pico-seconds, which is much shorter than the duration of the laser pulse (two nano-seconds). This means that the predicted equilibrium Raman spectrum is observable during the experiment. But it also suggests that the back-reaction on the Langmuir spectrum may be ignorable, at least for times of interest in this particular example.

C. Coherent radiation from relativistic electron beams

Recently, radiation has been detected at high harmonics of the plasma frequency during intense, relativistic beam-plasma laboratory experiments.[2] The reported spectrum is relatively flat, continuous (i.e., no spikes), and extends from ω_p out to at least 7 ω_p.

The lack of spikes in the spectrum may result from a broadband instability and/or source of radiation excited by the electron beam, having a range in frequencies on the order of ω_p. The theory could be genralized easily to include such a mechanism for injection near ω_p. We expect the beam to excite a linear instability at the fundamental, for example, via the parametric decay of a Langmuir wave into an ion-acoustic and a transverse wave.

However, to explain a flat spectrum out to at least 7 ω_p in the context of the present theory, we require a value of z at least on the order of unity.

$$z \equiv W/\gamma_d \geq 1.$$

The Langmuir energy density, W^L, is not measured in the experiment, so the parameter W is undetermined. To ensure the validity of the weak turublence theory used in this paper, W^L must be less than one. Therefore W is bounded above as follows (cf. Eq. (3b))

$$W \leq \frac{1}{8n} (v_e/c)^{2\alpha} ,$$

where α is less than 0.7, as explained in Sec. I.

If the dominant dissipation mechanism is assumed to be absorption at, or transmission through, the chamber walls, then $\nu_d = c/\omega_p R$, where R is the effective length of the chamber. In this case we estimate the following upper bound for z.

$$z \leq \frac{7}{80\pi} (v_e/c)^2 (\omega_p R/c)$$

Typical measured values of $(v_e/c)^2$ and ω_p are 10^{-5} and 10^{10} s^{-1}, respectively. It follows that R must be at least 4×10^4 m to give us a value of z that is greater than one and so to admit the present theory as an explanation of the observations. The value of R depends on the rate at which radiation is reflected by the chamber walls. If the walls do not reflect the radiation at all, then R is the actual chamber length (1 m in the experiment). In the limit of perfectly reflecting walls, R diverges ($\nu_d \to 0$); the plasma is infinitely long, in effect, and efficient up-scattering is possible. In fact ν_d is bounded away from zero by other dissipation mechanisms, such as collisional losses.

It is unlikely that the effective length of the chamber is as large as 10^4 times the actual chamber length, so it is doubtful that Raman scattering is responsible for producing the observed high-frequency radiation. It would be interesting, however, to compare experimental results for a variety of chamber wall coatings differing in reflectivity.

V. Unbounded Behavior

Here we briefly consider some interesting properties of unbounded behavior resulting from linear instability at the fundamental. With the addition of a growth rate at the fundamental ($\gamma_1 < 0$) it is possible for the energy density of the radiation to diverge in time, eventually reaching the nonlinear regime where the stimulated scattering plays an important role. As mentioned in Sec. IV, stimulated scattering tends to push the transverse spectrum back down to low frequencies and thus to decrease the net rate of dissipation. As the energy density diverges (Fig. (5a)) it does so faster than exponentially (Fig. (5b)) with an increasing fraction of the total energy at the fundamental (Fig. (5c)).

However, it is important to emphasize that even though the long-time behavior is unbounded, the spectrum may be acceptably stationary for some finite time of interest, depending on the particular problem. For example, if the source is pulsed (along with the growth rate) it may shut off before the stimulated scattering is activated.

There is a very interesting short-time behavior that is generally observed in these "unbounded" examples which dramatically illustrates the effect of the stimulated scattering on the evolution of the spectrum. In Fig. (5d) we see the linear evolution responsible for up-scattering the radiation to a mean frequency of just under $5\omega_p$ after about 0.7 seconds. (Except for the growth rate at the fundamental, parameters are similar to those in the corona example of Fig. (3).) At this point, the spectrum is as shown in Fig. (5e) and is on the

brink of activating the stimulated scattering. When it does so, the nonlinear terms push the radiation back down into the fundamental so that the average freqeuncy swings back down toward ω_p.

A growth rate at the fundamental does not necessarily produce unbounded behavior. The growth rate must be larger than a certain threshold value above which the linear instability cannot be saturated. The case depicted in Figs. (5) lies just above threshold. Of course the equilibria reached in spite of linear instability may lie well within the domain of the linearized kinetic equation. In this case, the linear analysis correctly predicts the characteristics of the spectrum. We emphasize that the shape of the spectrum is independent of the source and growth rate at the fundamental (see Eq. 12, for example), these serving only to determine the overall size (total energy density) of the spectrum.

IV. Concluding Remarks

We have obtained the stationary states of a linear kinetic equation that describes the scattering of a source of radiation by a Langmuir-turbulent plasma of finite spatial extent. Because the scattering proceeds via nearest-neighbor interactions only, it is straightforward to write the solution in terms of unending continued fractions. These fractions provide an efficient algorithm for calculating the equilibria as well as accurate approximations to those equilibria in terms of simple analytic functions. The generalization of this method to include the effects of nonlinear nearest-neighbor interactions (stimulated scattering) is currently under investigation.

Acknowledgements:

We would like to thank D. Pesme and F. Tappert for their discussions and assistance in this work.

This work was supported by the Air Force Office of Scientific Research (Grant No. 84-0007), the National Aeronautics and Space Administration (Grant No. NAGW-91), and the National Science Foundation, Atmospheric Sciences Section (Grant No. ATM-8020426). We also acknowledge the National Center for Atmospheric Research for computing time.

References:

1. K. Estabrook and W.L. Kruer, Phys. Fluids, 26, 1892 (1983).
2. K. Kato, G. Benford and D. Tzach, Phys. Rev. Lett. 50, 1584 (1983).
3. P.Y. Cheung, A.Y. Wong, C.B. Darrow and S.J. Qian, Phys. Rev. Lett. 48, 1848 (1982).
4. P. Leung, M.Q. Tran and A.Y. Wong, Plasma Physics 24, 567 (1982).
5. S.A. Colgate, E.P. Lee, and M.N. Rosenbluth, Astrophys. J. 162, 649 (1970).
6. S.A. Kaplan and V.N. Tsytovich, Plasma Astrophysics, Pergamon Press New York (1973).
7. D. Newman, "Stimulated Compton Conversion of Langmuir Waves by Ultra Relativistic Electron Beams," submitted for publication to Phys. Fluids.
8. C. Mercier and H. Rosenberg, Solar Phys. 39, 193 (1974).
9. V.N. Tsytovich, Theory of Turbulent Plasma, (Consultants Bureau, New York, 1977) p. 391.
10. W.B. Jones and W.J. Thron, Encyclopedia of Mathematics, (Addison-Wesley Publishing Company, Reading, Mass., Vol. 11, 1980), p. 183.
11. M. Abramowitz and I.A. Stegun, Handbook of Mathematical Functions, (Dover Publications, Inc., New York, 1972), p. 358.
12. S.A. Colgate, E.P. Lee, and M.N. Rosenbluth, Astrophys. J., 162, 649 (1970).
13. N.H. Burnett, H.A. Baldis, M.C. Richardson, and G.D. Enright, Appl. Phys. Lett., 31, 172 (1977).

Table I

n	a) Formula	b) Kinetic Equation
1	1.00	0.45
2	1.43	1.33
3	1.65	1.61
4	1.81	1.78
5	1.92	1.91
6	2.01	2.00
7	2.09	2.08
8	2.15	2.15
9	2.21	2.21
10	2.26	2.26
11	2.30	2.30

Table I:

$-\log_{10}[U_{n+1}/U_n]$ vs n for a) the approximation to the spectrum given by eq. (16), and b) the long-time asymptotic solution of linearized Eq. (3a). $z = 10^{-1}$ and physical parameters are given in the caption to Fig. 4. The absolute error in both columns is ± 0.005.

Figure Captions:

1) Diagrams of Raman scattering. k denotes photons; q denotes Langmuir waves.

2) The (one-dimensional) Langmuir wave spectrum that we assume. W_q^L = (energy density of Langmuir waves at q)/($4\pi n_o T_e$).

3) U_n vs n for parameters appropriate for a hypothetical stellar corona with a higher level of Langmuir turbulence than is observed for the solar corona. $T_e = 10^2$ eV, $\omega_p = 6\times10^7$/sec, $4\pi n_o T_e = 2\times10^{-3}$ erg/cm^3, R = 10^9 m, $z = 10^3$, $\nu_d = 5\times10^{-9}$, S = 100, $\alpha W^L = 0.7$.

4) $\text{Log}_{10}[U_n/U_1]$ vs n for the parameters of the laser-target interaction experiment of Burnett et al.[13] Crosses indicate their results. $T_e = 10^4$ eV, $\omega_p = 1.78\times10^{14}$/sec, $4\pi n_o T_e = 2\times10^5$ Joules/cm^3, $z = 10^{-1}$, $R = 3\times10^{-2}$ cm, $\nu_d = 5.6\times10^{-3}$, S = 638, $\alpha W^L = 0.7$.
   a) Linearized kinetic equation prediction.
   b) Full kinetic equation prediction, including stimulated scattering.

5) Unbounded behavior resulting from linear instability at ω_p.
   a) Total, dimensionless energy density ($\sum_n U_n$) vs. time.
   b) The logarithmic derivative of the total number density, $U_n \div n$, vs. time, i.e., an effective growth rate.
   c) The fraction of the total energy density that is at ω_p vs. time.
   d) The average frequency, $\sum U_n/[\sum U_n/n]$, vs. time.
   e) The spectrum at the time at which the up-scattering is greatest.

$T_e = 10^2$ eV, $\omega_p = 6\times10^7$/sec, $4\pi n_o T_e = 2\times10^{-3}$ erg/cm^3,
$R = 10^8$ m, $z = 10^2$, $\nu_1 = -37.5\times10^{-8}$, $\nu_d = 5\times10^{-8}$, $S = 10$,
$\alpha W^L = 0.7$.

Appendix A: Reduction of the Golden-Rule Kinetic Equation to One-Dimension

In terms of number densities for the transverse and longitudinal spectra,

$$\frac{\langle |E_k^T|^2 \rangle}{8\pi\hbar\omega_k V} \equiv n_k$$

and

$$\frac{\langle |E_q^L|^2 \rangle}{8\pi\hbar\omega_p V} \equiv n_q^L \quad ,$$

the well-known kinetic equation[9] for the scattering processes described in Fig. 1 is

$$\dot{n}_k = \int \frac{d^3q}{(2\pi)^3} \cdot \left\{ |M^-|^2 \delta(\omega_k - \omega_{k-q} - \omega_p) \underset{①}{[-n_k n_q^L} \underset{③}{+ n_{k-q} n_q^L} \underset{⑤}{- n_k n_{k-q}}] + \right.$$
$$\left. + |M^+|^2 \delta(\omega_k - \omega_{k+q} + \omega_p) \underset{②}{[-n_k n_q^L} \underset{④}{+ n_{k+q} n_q^L} \underset{⑥}{+ n_k n_{k+q}}] \right\} \quad , \qquad \text{(A1)}$$

where

$$|M^\pm|^2 \equiv \pi^2 \left(\frac{e}{m_e}\right)^2 \frac{\hbar\omega_p}{\omega_k \omega_{k\pm q}} q^2 \quad .$$

Here we neglect the thermal dispersion of Langmuir waves in using ω_p alone for their frequency. The polarization factors usually present in the matrix elements, $|M^\pm|^2$, have been taken to be a constant and are suppressed. That is, we assume an unpolarized source. In Eq. (A1) we are also suppressing the vector notation on the wave vectors $\underline{k}$ and $\underline{q}$. Terms ① through ④ give us the linearized kinetic equation; terms ⑤ and ⑥ provide the stimulated scattering. (Notice that we have defined Fourier transforms in an arbitrarily large cube in x-space of volume V so that $|E_k^T|^2$ and $|E_q^L|^2$ have the dimensions of energy·volume.)

We assume that both the Langmuir and transverse spectra are strongly peaked about a single direction in k-space and calculate narrow-angle averages of the number densities about that direction. The result is expressed in terms of the transverse wave number density as a function of frequency,

$$N(\omega_k) \equiv \int_{\Delta\Omega_k} n_k \frac{d^3k}{d\omega_k} \quad .$$

For example, consider term ④ in Eq. (A1). Integrating over $\Delta\Omega_k$, we have

$$\int_{\Delta\Omega_k} d\Omega_k \, ④ \sim \int d^3q \, \frac{q^2}{\omega_k} \, n_q^L \int_{\Delta\Omega_k} d\Omega_k \, \frac{n_{k+q}}{\omega_{k+q}} \, \delta(\omega_k - \omega_{k+q} + \omega_p) \quad .$$

To perform the integration over $\Delta\Omega_k$, define

$$\underline{\xi} \equiv \underline{k}+\underline{q} \ ,$$

and assume that the only contribution to the integral comes from a very narrow neighborhood of $\theta_\xi = 0$; see Fig. 6. Then, ignoring the variation $|\underline{\xi}|$ that results from a variation in θ_k, we have

$$\xi d(\cos\theta_\xi) \tilde{=} k d(\cos\theta_k)$$

from $\underline{q}\cdot\underline{\xi} = q^2 + \underline{k}\cdot\underline{q}$. So the integral over $\Delta\Omega_k$ is approximated by

$$\frac{\xi}{k\omega_\xi} \, \delta(\omega_k - \omega_\xi + \omega_p) \int_{\Delta\Omega_\xi} d\Omega_\xi \, n_\xi \quad ,$$

and we have

$$\int_{\Delta\Omega_k} d\Omega_k \, ④ \sim \int d^3\xi \, |\underline{\xi}-\underline{k}|^2 \, \frac{\xi}{k\omega_k\omega_\xi} \, n^L_{\underline{\xi}-\underline{k}} \, \eta(\xi) \, \delta(\omega_k - \omega_\xi + \omega_p) \quad .$$

Here $\eta(\xi) \equiv \int_{\Delta\Omega_\xi} d\Omega_\xi n_\xi$ and is a function of $|\underline{\xi}|$ only; $d^3\xi = d^3q$, now, with $\underline{k}$ fixed. Integrating over the δ-function in ω_ξ, and using

$$\delta(\omega_k-\omega_\xi+\omega_p) = \delta(\xi-\xi^*)\,\frac{\omega_{\xi^*}}{c^2\xi^*}$$

where $c^2(\xi^*)^2 \equiv (\omega_k+\omega_p)^2 - \omega_p^2$, leaves us with

$$\int \textcircled{4} d\Omega_k \sim \eta(\xi^*)\,\frac{(\xi^*)^2}{c^2 k\omega_k}\int d\Omega_{\xi^*}\,|\underline{\xi}^*-\underline{k}|^2\, n^L_{\underline{\xi}^*-\underline{k}} \quad .$$

From

$$(k\cdot\xi^*)\cos\theta_{\xi^*} - k^2 = k|\underline{\xi}^*-\underline{k}|\cos\theta_{\underline{\xi}^*-\underline{k}} \quad ,$$

and neglecting $d(|\underline{\xi}^*-\underline{k}|)$, we have

$$d(\cos\theta_{\xi^*}) \simeq \frac{|\underline{\xi}^*-\underline{k}|}{\xi^*}\, d(\cos\theta_{\underline{\xi}^*-\underline{k}})$$

or

$$d\Omega_{\xi^*} \simeq \frac{|\underline{\xi}^*-\underline{k}|}{\xi^*}\, d\Omega_{\xi^*-\underline{k}} \quad .$$

Thus

$$\int \textcircled{4} d\Omega_k \sim \frac{\eta(\xi^*)(\xi^*)^2}{c^2 k\omega_k \xi^*}\int d\Omega_{\underline{\xi}^*-\underline{k}}\,|\underline{\xi}^*-\underline{k}|^3\, n^L_{\underline{\xi}^*-\underline{k}}$$

The contribution to $\dot{N}(\omega_k)$ is obtained after multiplying this expression by

$$k^2/V_g(k) \quad ,$$

where $V_g(k) \equiv d\omega_k/dk$.

Using

$$V_g(k)\,\frac{\omega_k}{k} = V_g(\xi^*)\,\frac{\omega_{\xi^*}}{\xi^*} = c^2 \quad ,$$

we have finally

$$\dot{N}(\omega_k) \sim \frac{\eta(\xi^*)(\xi^*)^2}{c^2 V_g(\xi^*)\omega_{\xi^*}}\int d\Omega_{\underline{\xi}^*-\underline{k}}\,|\underline{\xi}^*-\underline{k}|^3\, n^L_{\underline{\xi}^*-k} \quad ,$$

or

$$\frac{1}{8\pi}\left(\frac{e}{m_e}\right)^2 \frac{\hbar\omega_p}{c^2} \frac{N(\omega_{\xi^*})}{\omega_{\xi^*}} |\xi^*-\underline{k}|^3 \int_{\Delta\Omega_{\underline{\mu}}} d\Omega_{\underline{\mu}}\, n_{\underline{\mu}}^L$$

as the contribution that term ④ makes to $\dot{N}(\omega_k)$.

Using the same tricks to evaluate the remaining five terms and assuming that

$$\hat{W} \equiv \int_{\Delta\Omega_{\underline{\mu}}} d\Omega_{\underline{\mu}}\, n_{\underline{\mu}}^L$$

is independent of $|\underline{\mu}|$ over

$$\frac{\omega_p}{c} \leq |\underline{\mu}| \leq \sqrt{3}\,\frac{\omega_p}{c}$$

we arrive at the following kinetic equation:

$$\dot{N}(\omega_k) + \frac{m}{c^2}\hat{W}\left[|k-\xi^+|^3 + |k-\xi^-|^3 H(\omega_k-2\omega_p)\right]\frac{N(\omega_k)}{\omega_k}$$

$$= \frac{m}{c^2}\hat{W}\left[|k-\xi^-|^3 \frac{N(\omega_k+\omega_p)}{(\omega_k+\omega_p)} + |k-\xi^-|^3 H(\omega_k-2\omega_p)\frac{N(\omega_k-\omega_p)}{(\omega_k-\omega_p)}\right] +$$

$$+ m\frac{N(\omega_k)}{\omega_k}\left[|k-\xi^+|^2 \frac{N(\omega_k+\omega_p)}{(\omega_k+\omega_p)} - |k-\xi^-|^2 H(\omega_k-2\omega_p)\frac{N(\omega_k-\omega_p)}{(\omega_k-\omega_p)}\right]$$

where H is the step function,

$$|k-\xi^{\pm}| \equiv \frac{1}{c}\left|(\omega_k^2-\omega_p^2)^{\frac{1}{2}} - [(\omega_k\pm\omega_p)^2-\omega_p^2]^{\frac{1}{2}}\right| ,$$

and

$$m \equiv \frac{1}{8\pi}\left(\frac{e}{m_e}\right)^2 \hbar\omega_p = \frac{\hbar\omega_p}{8\pi}\left(\frac{\omega_p^2 v_e^2}{4\pi n_o T_e}\right) .$$

$N(\omega_k)$ has the dimensions of (time)/(length)^3.

Introducing

$$n \equiv \omega_k/\omega_p ,$$

a dimensionless energy density

$$U(n) \equiv 2\hbar\omega_k \omega_p \frac{N(\omega_k)}{8\pi n_o T_e} \quad ,$$

and measuring time in units of ω_p^{-1}, the kinetic equation is written in the following dimensionless form:

$$\dot{U}(n) = -W[A^3+HB^3]\, U(n)/n +$$

$$+ W[A^3 \frac{n}{(n+1)^2} U(n+1) + HB^3 \frac{n}{(n-1)^2} U(n-1)]$$

$$+ V \frac{U(n)}{n} [A^2 \frac{U(n+1)}{(n+1)^2} - HB^2 \frac{U(n-1)}{(n-1)^2}] \quad , \qquad (A2)$$

where

$$W \equiv \frac{\hbar\omega_p}{8\pi} \frac{\hat{W}}{4\pi n_o T_e} (\frac{v_e}{c})^2 (\frac{\omega_p}{c})^3$$

$$V \equiv \frac{1}{8\pi} (\frac{v_e}{c})^2$$

and

$$A_{(+)}, B_{(-)} \equiv \left|(n^2-1)^{\frac{1}{2}} - [(n\pm1)^2-1]^{\frac{1}{2}}\right| \quad .$$

Recapitulating:

$$U(n) \equiv \frac{\omega_p}{4\pi n_o T_e} \hbar\omega_k N(\omega_k) = \frac{\omega_p}{4\pi n_o T_e} \int_{\Delta\Omega_k} \hbar\omega_k n_k \frac{k^2}{V_g(k)} d\Omega_k$$

$$= \frac{\omega_p}{4\pi n_o T_e} \int_{\Delta\Omega_k} \frac{\langle|E_k|^2\rangle}{8\pi V} \frac{k^2}{V_g(k)} d\Omega_k$$

Dissipation will add a term to the right-hand-side of Eq. (A2):

$$-2\gamma(n)\cdot U(n) \quad ,$$

where $-2\gamma(n)$ is the rate at which transverse energy is removed from the system, normalized to the electron plasma frequency. A source of radiation at k will add

a term to the RHS of Eq. (A2):

$$S(n) = \frac{1}{4\pi n_o T_e} \int_{\Delta\Omega_k} \hbar\omega_k \, S_k \, \frac{k^2}{V_g(k)} \, d\Omega_k \quad .$$

(Note, $k = k(n)$ here.)

Thus, we arrive at Eq. (3a).

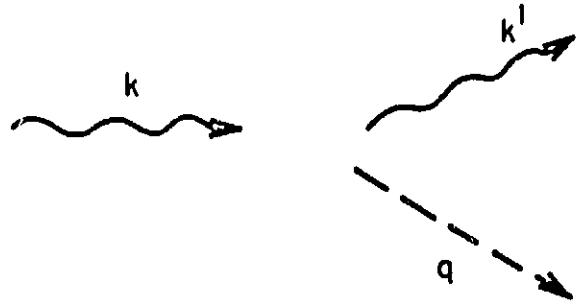

+

Fig. 1

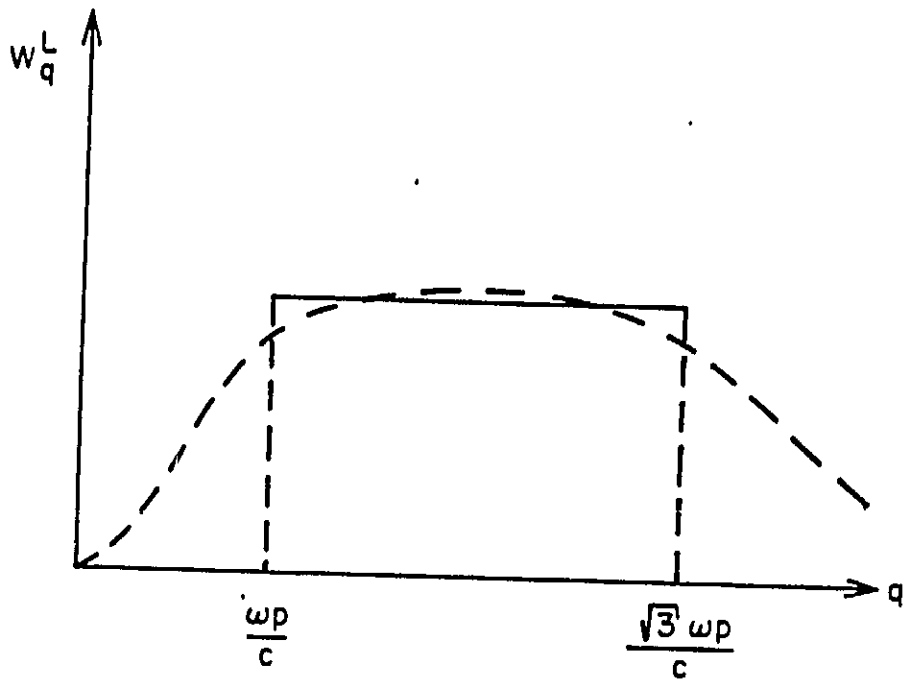

Fig. 2

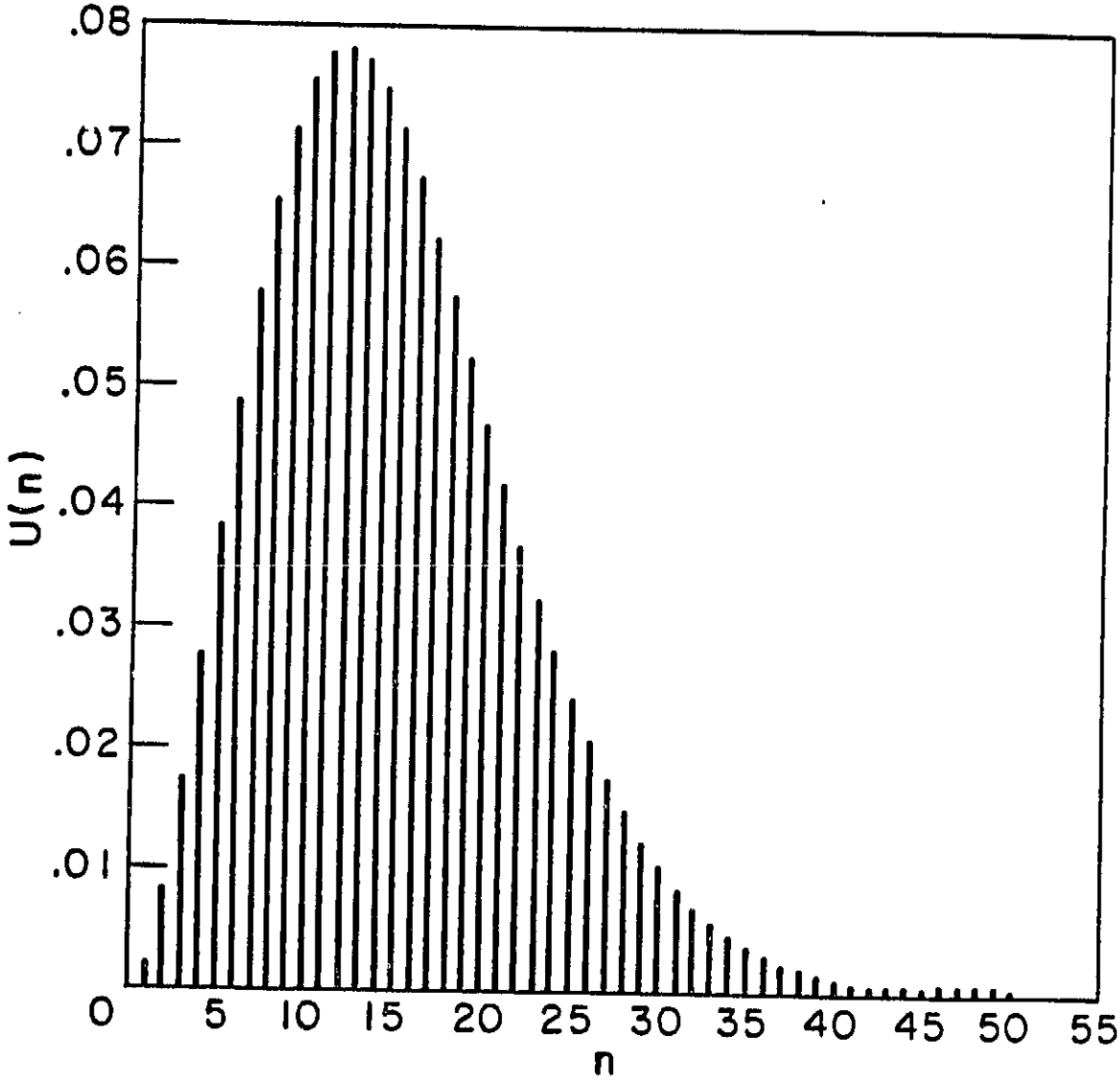

Fig. 3

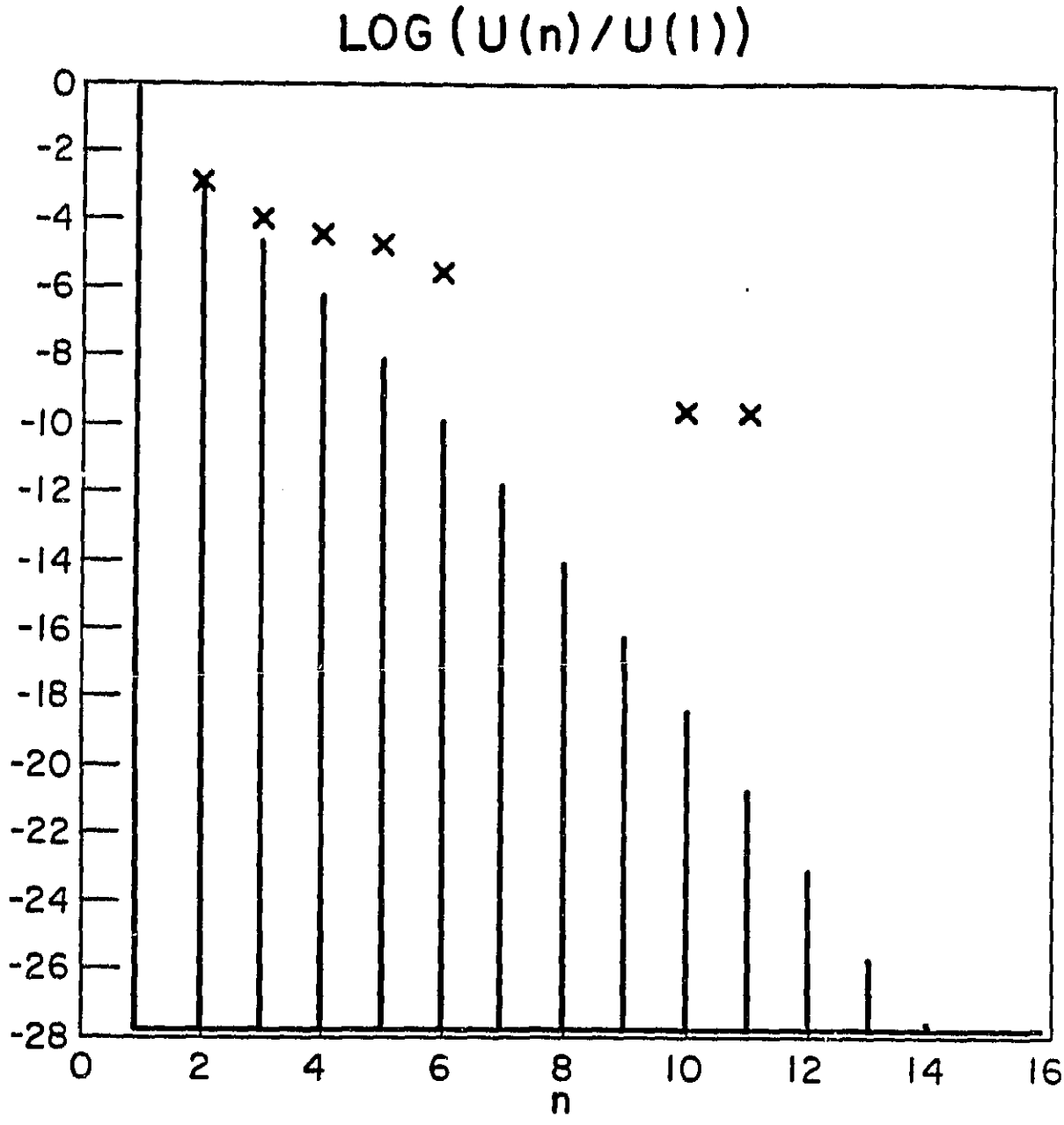

Fig. 4a

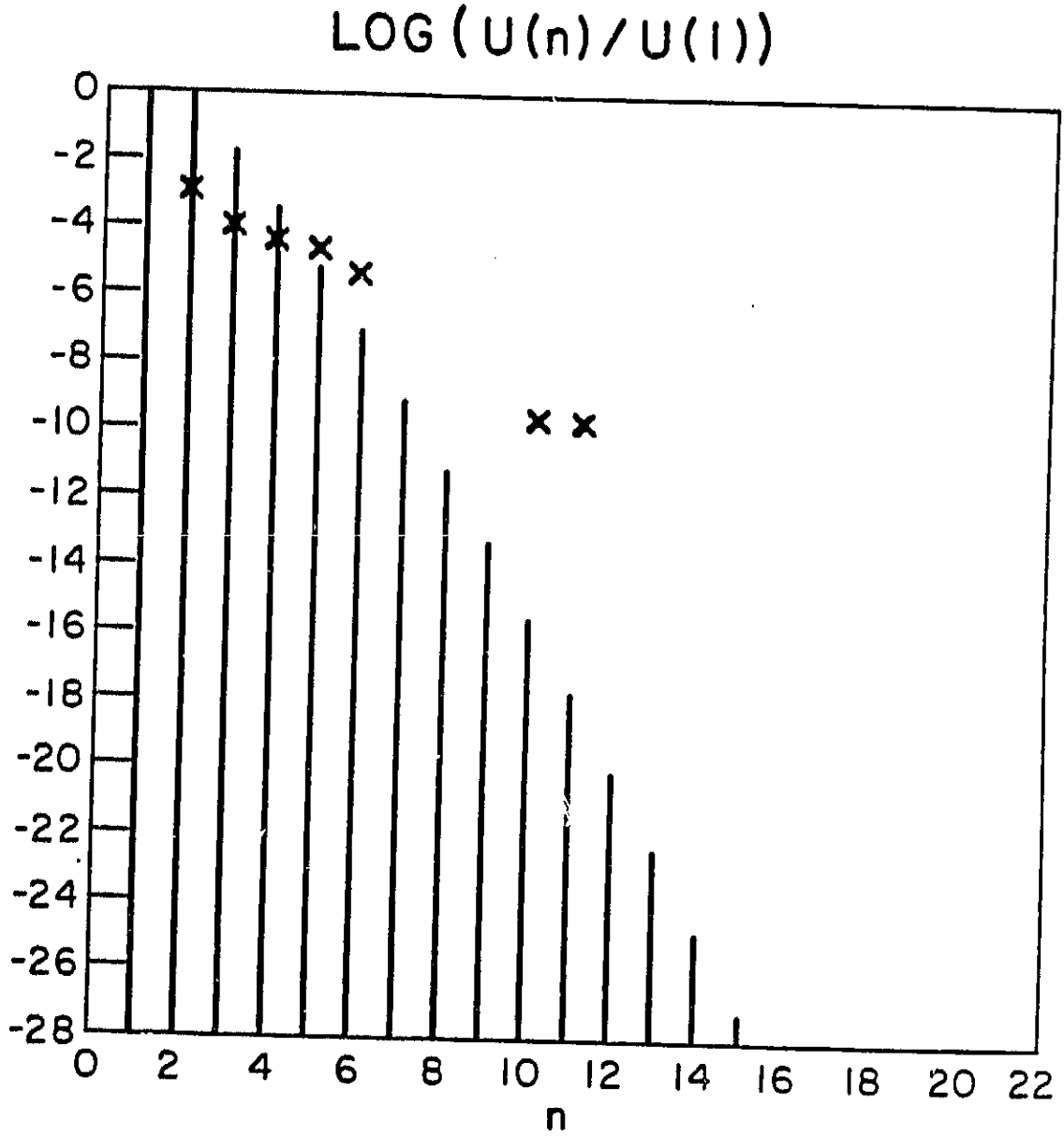
LOG (U(n) / U(1))
0
-2
-4
-6
-8
-10
-12
-14
-16
-18
-20
-22
-24
-26
-28
0
2
4
6
8
10
12
14
16
18
20
22
n

Fig. 4b

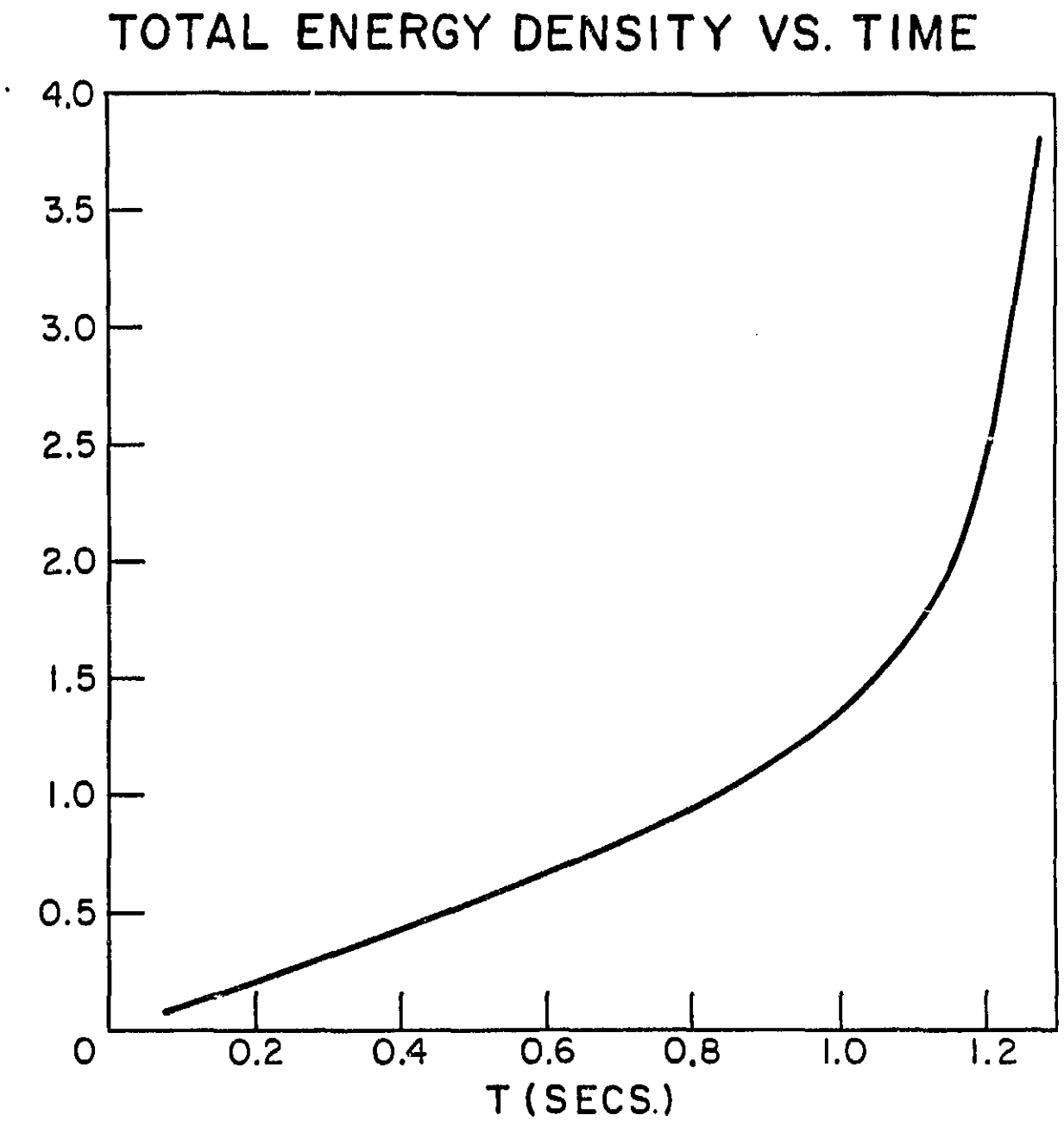
TOTAL ENERGY DENSITY VS. TIME
4.0
3.5
3.0
2.5
2.0
1.5
1.0
0.5
0
0.2
0.4
0.6
0.8
1.0
1.2
T (SECS.)

Fig. 5a

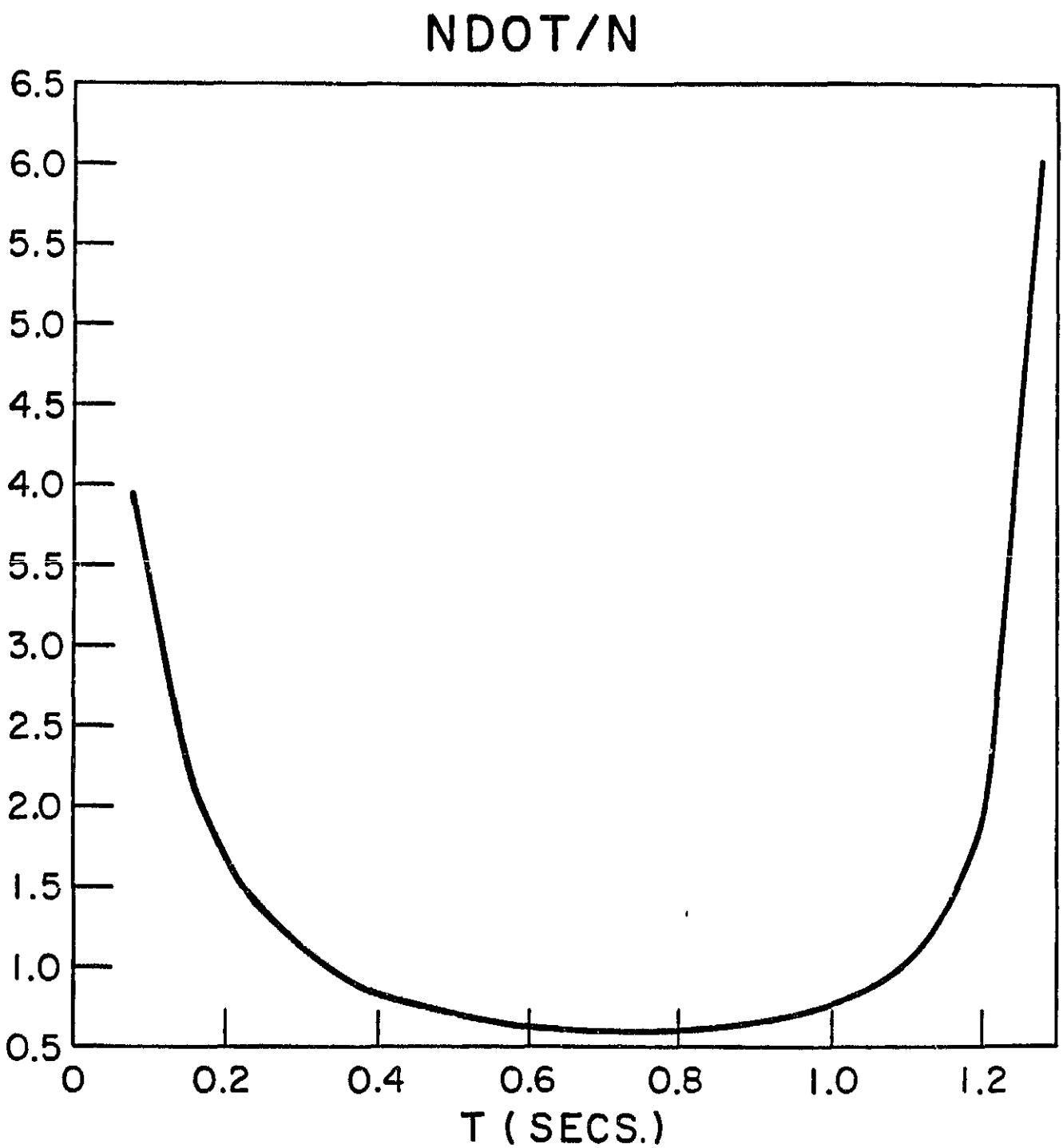

Fig. 5b

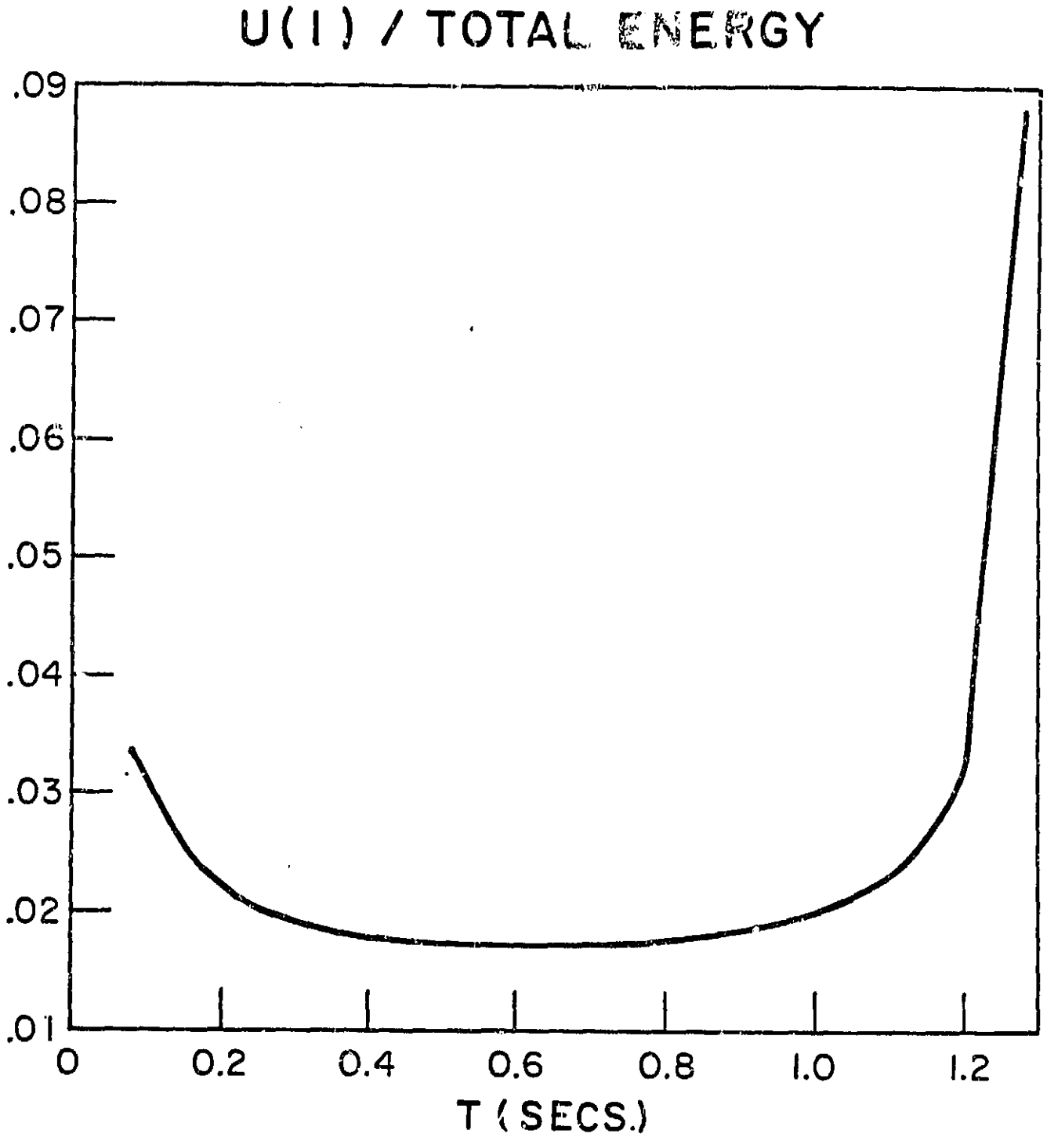

Fig. 5c

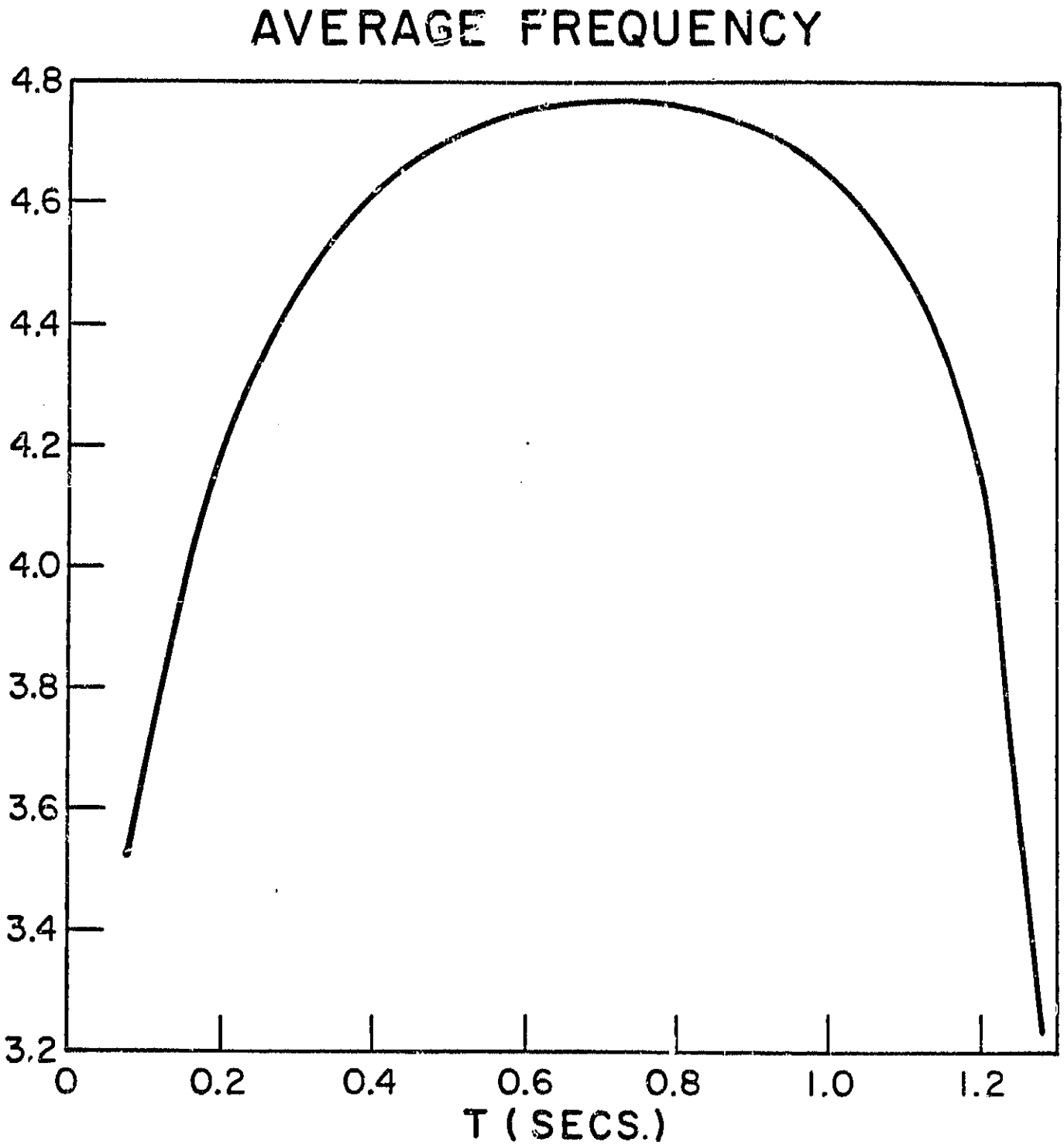
AVERAGE FREQUENCY
4.8
4.6
4.4
4.2
4.0
3.8
3.6
3.4
3.2
0
0.2
0.4
0.6
0.8
1.0
1.2
T (SECS.)

Fig. 5d

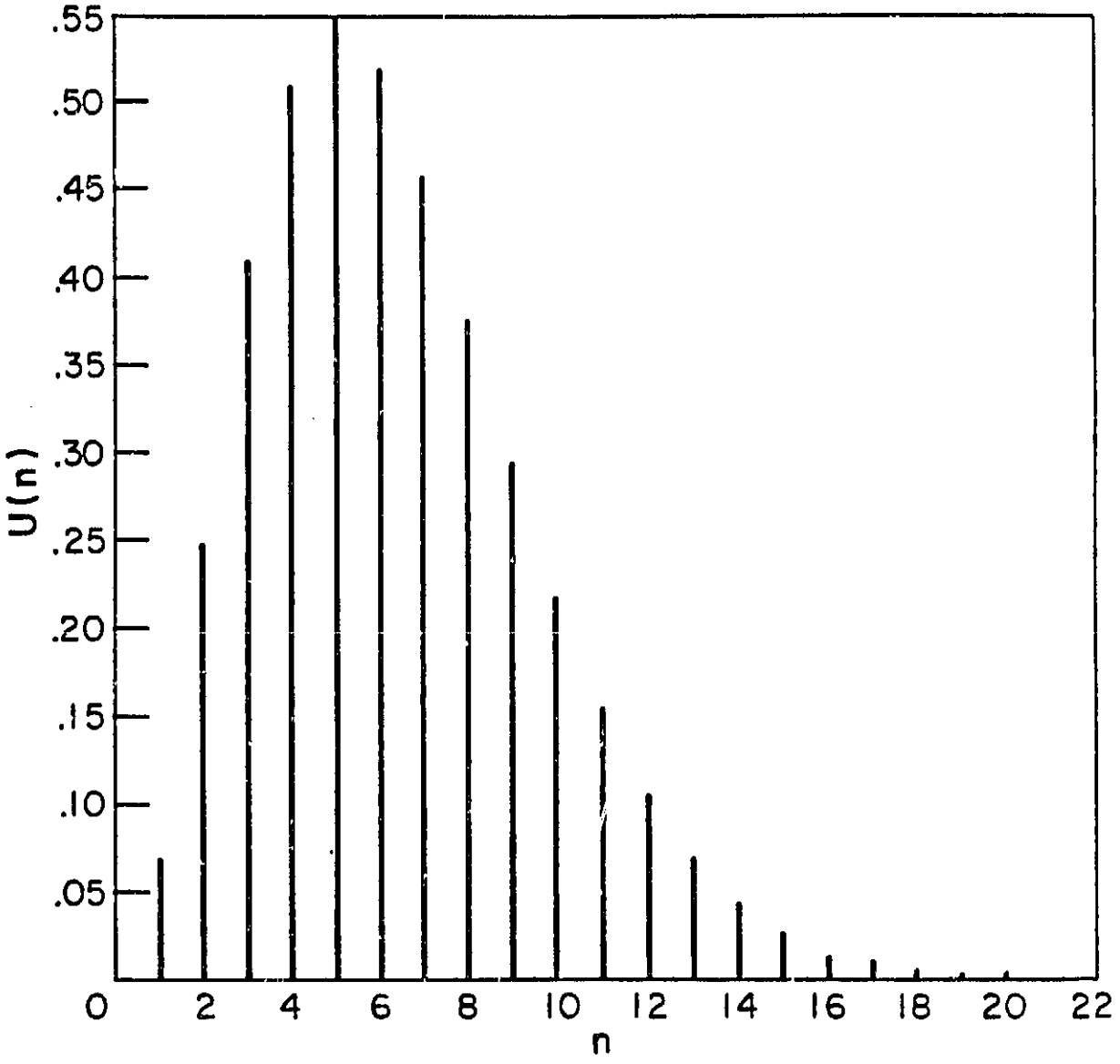

Fig. 5e

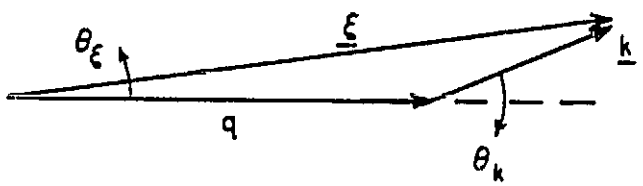

Fig. 6